CHALMERS
UNIVERSITY OF TECHNOLOGY

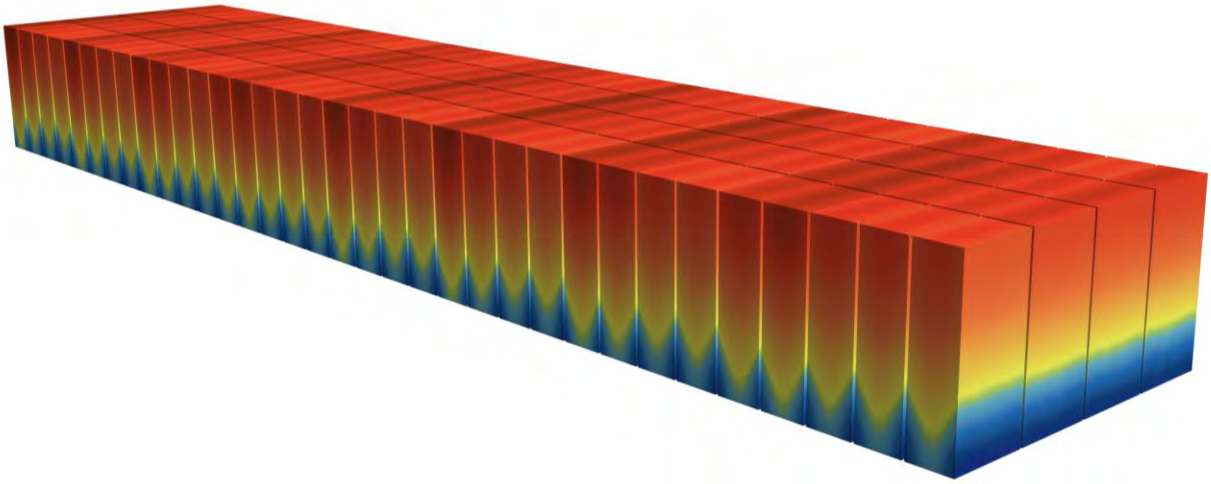

Automatic Optimisation of a Battery Pack Cooling Plate

Master's thesis in Applied Mechanics

Kevin Eide
Albert Lundgren

DEPARTMENT OF MECHANICS AND
MARITIME SCIENCES

CHALMERS UNIVERSITY OF TECHNOLOGY
Gothenburg, Sweden 2022
www.chalmers.se

MASTER'S THESIS IN APPLIED MECHANICS

Automatic Optimisation of a Battery Pack Cooling Plate

KEVIN EIDE
ALBERT LUNDGREN

Department of Mechanics and Maritime Sciences
Division of Fluid Dynamics
CHALMERS UNIVERSITY OF TECHNOLOGY

Göteborg, Sweden 2022

Automatic Optimisation of a Battery Pack Cooling Plate
KEVIN EIDE
ALBERT LUNDGREN

Master's thesis 2022:20
Department of Mechanics and Maritime Sciences
Division of Fluid Dynamics
Chalmers University of Technology
SE-412 96 Göteborg
Sweden
Telephone: +46 (0)31-772 1000

Cover:
A temperature plot of the battery pack is shown on the front cover.

Chalmers Reproservice
Göteborg, Sweden 2022

Automatic Optimisation of a Battery Pack Cooling Plate
Master's thesis in Applied Mechanics
KEVIN EIDE
ALBERT LUNDGREN
Department of Mechanics and Maritime Sciences
Division of Fluid Dynamics
Chalmers University of Technology

Abstract

Electric vehicle adoption is on the rise which introduces a need for effective battery pack cooling systems. Effective cooling systems play a key role in the battery packs service life. This thesis compares two indirect liquid-cooled cooling configurations and optimises the cooling system in terms of maximum battery cell temperature difference, maximum battery cell temperature and pressure drop. The analysed part of the cooling system consists of aluminium plates with channels, where coolant flows through. One configuration consisting of one large cooling plate and the other of multiple cooling plates.

The heat transfer from the battery pack to the coolant was simulated using the commercial computational fluid dynamics (CFD) solver Star-CCM+. Using CFD each battery cells temperature was monitored to evaluate the efficiency of the cooling system. The optimisation involved varying the geometry of the cooling plate channels to study its effect on the heat transfer.

The study found that placing cooling plates between the battery cells, rather than placing a single large plate under the battery cells, yielded substantially lower battery cell temperature differences and battery cell maximum temperatures. This is attributed to the interface area having a large effect on the heat transfer and the length of the channels having a large effect on the temperature difference and pressure drop. While using multiple plates the maximum battery cell temperature was decreased by 21.4 K and the temperature difference was 0.452 K lower. Several channel designs were tested based on the results to further improve the multiple cooling plate configuration. The temperature difference and maximum temperature was further reduced by 0.066 K and 0.634 K respectively.

Keywords: Battery, Lithium ion, BTMS, Thermal Management, CFD, Heat transfer, EV, Battery Degradation, Liquid cooled, Cooling plate

Contents

Abstract **i**

Contents **iii**

Preface **v**

1 Introduction **1**
1.1 Lithium-ion battery . . . 1
1.1.1 Battery degradation . . . 2
1.1.2 Thermal runaway . . . 2
1.2 Battery thermal management system . . . 2
1.3 Aim: . . . 2
1.4 Limitations: . . . 3
1.5 Ethical considerations . . . 3

2 Theory **4**
2.1 Computational fluid dynamics . . . 4
2.2 Reynolds Number . . . 5
2.3 Boundary layer . . . 5
2.4 Thermodynamics . . . 6
2.4.1 Energy Balance . . . 6
2.5 Pressure drop . . . 7
2.6 Temperature variance . . . 7
2.7 Battery modelling . . . 7
2.8 Battery thermal management system . . . 8
2.8.1 Air-cooled system . . . 8
2.8.2 Liquid-cooled system . . . 8
2.8.3 PCM cooled system . . . 9

3 Method **10**
3.1 Geometry . . . 10
3.1.1 Large cooling plate . . . 12
3.1.2 Multiple cooling plates . . . 12
3.1.3 Interfaces and contact resistance . . . 13
3.2 Models and materials . . . 13
3.3 Mesh . . . 15
3.4 Boundary conditions . . . 16
3.5 Post-Processing . . . 16
3.6 Automatic Optimisation . . . 17
3.7 Transient simulations . . . 17
3.8 Further Processing of Multiple Plates Configuration . . . 18
3.8.1 Wider Triple U design . . . 18
3.8.2 Wider Triple U design With Fins . . . 18
3.8.3 Five U design . . . 19
3.8.4 Single U Channel . . . 19

4 Result **20**
4.1 Large cooling plate . . . 20
4.2 Multiple cooling plates . . . 21
4.3 Processing of the Multiple Plates Configuration . . . 23
4.4 Increasing Inlet Temperatures . . . 24
4.5 Changing the anisotropic thermal conductivity of the battery cells . . . 24
4.6 Transient simulations . . . 25
4.6.1 Maximum power output, maximum battery strain . . . 25

4.6.2 Halved power output . . . 26
4.6.3 Crisis simulation, critical temperature . . . 26
4.7 Mesh Independence Study . . . 27

5 Discussion **28**
5.1 Comparing the two cooling configurations . . . 28
5.2 Further Processed Multiple Plate Designs . . . 31
5.3 Transient simulations . . . 34
5.4 Evaluating the best design . . . 35
5.5 Limitations of the used battery cell design . . . 36
5.6 Automatic Optimisation & Methodology . . . 36
5.7 Limitations of the study . . . 36

6 Conclusion **37**
6.1 Future Work: . . . 37
References . . . 38

A Mesh Study **I**

B Study of Wall y+ **III**

Preface

This study, consisting mainly of CFD evaluations of different cooling designs for an EV battery pack, has been carried out from January 2022 to June 2022. The project which attributes to 30 ECTS points is a master thesis concerning fluid dynamics and heat transfer. The project was carried out jointly at FS Dynamics in their Gothenburg office and at the Department of Mechanics and Maritime Sciences at the Division of Fluid Dynamics at Chalmers University of Technology, Gothenburg.

The project has been carried out with the much appreciated help of our supervisor at FS Dynamics, Specialist Engineer CFD, Robert Rundqvist. Robert was available for help every day and every week and was always very pedagogical and professional.

We would also like to thank our examiner at Chalmers, Professor Henrik Ström, for taking us under his wing.

Finally, we would also like to thank all of our co-workers in the office for the help we have received and for making us feel right at home from day one.

Göteborg, Sweden 2022
KEVIN EIDE
ALBERT LUNDGREN

Notations

ΔT always refers to the temperature difference of the hottest and the coldest battery cell, if not specified otherwise.

Abbreviations

CFD	Computational Fluid Dynamics
EV	Electric Vehicle
ICEV	Internal combustion engine vehicle
BTMS	Battery Thermal Management System
PCM	Phase change material
$k-\omega$	k-ω-SST turbulence model
$k-\epsilon$	k-ϵ turbulence model
RANS	Reynolds Averaged Navier Stokes

Parameters

ΔT	Temperature Difference
ΔP	Pressure Drop
V	Average velocity
L	Characteristic length scale
D	Hydraulic diameter
Q	Volume flow
$\dot{Q}$	Rate of heat flow
u^*	Friction velocity
τ_w	Wall shear stress
ρ	Density
μ	Dynamic viscosity
ν	Kinematic viscosity
f	Friction factor
Re	Reynolds number
u	Velocity in the Overlap layer
u^+	Non-dimensional velocity
y	Wall distance
y^+	Non-dimensional Wall distance
q	Heat transfer
k	Thermal conductivity
A	Area
R_c	Thermal contact resistance
$\dot{m}$	Mass flow rate
c_p	Specific heat capacity

1 Introduction

An electric vehicle (EV) is a vehicle that makes use of stored chemical energy in a battery pack, to power its electrical motors in order to propel the vehicle. When the batteries have been discharged they can be charged through a power outlet on the vehicle. The most common battery type for electric vehicles today is lithium-ion batteries.

EVs are widely regarded as more efficient and environment-friendly compared to internal combustion engine vehicles (ICEV) [1]. The transition from ICEV to EV in the transportation sector has the potential to reduce the emissions of greenhouse gases CO_2 by up to 80 % [1]. Additional environmental benefits of EVs are reduced particle emissions in densely populated urban areas, resulting in increased air quality and reduced risk of smog [2]. The market for EVs is predicted to grow rapidly due to consumers increasing environmental concerns and EVs decreasing purchase costs [3]. Costs still being the main reason for consumers hesitance to buy an EV [4].

Additionally, regulations are being proposed and passed in the western world that ban sales of new ICEVs [3], forcing car manufacturers to develop alternative propulsion systems, where EVs are currently considered the best option. In this race to develop better EVs, mainly large capacity EVs that charge and discharge their batteries faster, large market shares are at stake for many companies. Charging and discharging the batteries heats the internal components of the battery pack, mainly due to the internal resistances of the individual battery cells [5]. This introduces a need for an efficient cooling system, often referred to as the *battery thermal management systems*, BTMS for short. The output range of a typical fast-charging station ranges from 50 kW to 350 kW [6].

The BTMS must have sufficient thermal management for a full charge at the rated charge power. The running costs associated with the BTMS are usually a pump or fan depending on the configuration. If the temperature in the battery gets too high it runs the risk of a thermal runaway where the battery starts to melt causing violent fires [5]. Sometimes this can be associated with the release of toxic gases which are harmful to the environment and humans.

For these reasons, FS Dynamics have requested an effective cooling system for EVs and a methodology which can decrease the time and cost associated with the development of new cooling systems for EVs.

1.1 Lithium-ion battery

A lithium-ion battery is a rechargeable battery widely used in electric vehicles and other portable electric devices. When a lithium-ion battery discharges, i.e. generate electricity, lithium-ions move from the anode to the cathode via the electrolyte. The reverse process happens as the battery is being charged [7]. For larger applications, the lithium-ion batteries are connected in series in a battery pack rather than making one very large battery [8]. Because batteries have an internal resistance the batteries also generate heat when they charge and discharge.

The optimal operating temperature range of lithium-ion batteries is 15-35 °C [9]. At higher temperatures, ranging from 35-60 °C, the wear of the batteries is accelerated [10]. When the temperature rises even further, 60+ °C, the battery runs the risk of a catastrophic failure called thermal runaway [5]. The aim is therefore to keep the temperature in the battery pack within the optimal range, and the temperature distribution even to minimize uneven wear.

1.1.1 Battery degradation

Repeated charging and discharging of the battery causes the electrolyte to thermally decompose and become chemically reduced [10], [11]. Chemical reduction causes ions of the electrolyte to react with the anode, decreasing the amount of ions present in the electrolyte. The resulting compound also sticks to the anode, decreasing the efficiency of the anode. At higher temperatures the electrolyte will also thermally decompose at both the anode and the cathode, forming thin layers of less and non-conducting compounds [10], [11]. The decomposition and reduction process is irreversible, i.e. as it occurs free ions become spent and can not be recovered. By also decreasing the efficiency of the anode and cathode the internal resistance is increased, meaning more heat generation per electrical current. Higher temperatures hasten the thermal decomposition further degrading the battery. Battery degradation plays a key role in the life span of the battery. By keeping the temperatures low in the battery, battery degradation can be alleviated by reducing the amount of thermal decomposition taking place.

1.1.2 Thermal runaway

A thermal runaway is a process that occurs when the battery cell becomes overheated, above its critical temperature. The critical temperature is an estimation of a temperature where the battery is prone to suffer a thermal runaway. Overheating of the cell leads to its components breaking down in exothermic reactions, further increasing the temperature of the cell [5]. This causes even more reactions to take place, leading to even higher temperatures. In an encapsulated battery with little to no venting, this will eventually lead to an explosion or a fire [12]. Thermal runaways can be avoided by not letting the battery reach its critical temperature, i.e having sufficient cooling. A thermal runaway can also be mitigated by venting the hot gases produced by the exothermic reactions.

1.2 Battery thermal management system

To ensure even temperature distribution in the battery pack, and to make sure the temperature does not get too high, a BTMS is implemented. The BTMS consists of a cooling system, insulation of the battery pack and regulates the temperature in the battery pack through sensors and controls [13]. The cooling system can be air-cooled or liquid-cooled. Ducts or cooling channels can be passed through the battery pack, either around or through the individual battery cells [13].

1.3 Aim:

The aim of this project is to compare the cooling performance of two liquid-cooled cooling configurations and to develop a methodology for automatically optimising the design.

The first cooling configuration consists of a single cooling plate with cooling channels, which the battery pack is placed on top of. The other configuration is a design where cooling plates are placed between every other row of battery cells, as illustrated in figure 1.1. The red rectangles are battery cells and the blue rectangles are the cooling plates, the red arrows illustrate heat transfer.

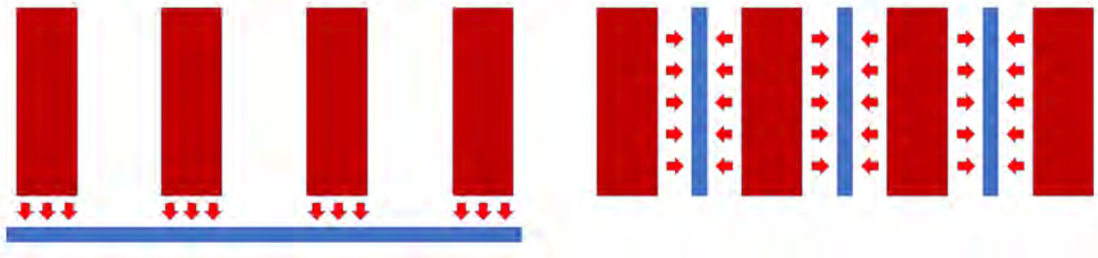

Figure 1.1: The two cooling configurations

A methodology will also be developed which involves varying parameters, simulating the design and evaluating the result automatically to yield the best design, as illustrated in figure 1.2. The parameters to be varied are geometrical parameters and the inlet velocity of the coolant. This is done to maximize the cooling performance by minimizing the temperature difference in the battery pack and the maximum cell temperature, as well as the pressure losses. User input is an initial design and the result is the optimal design.

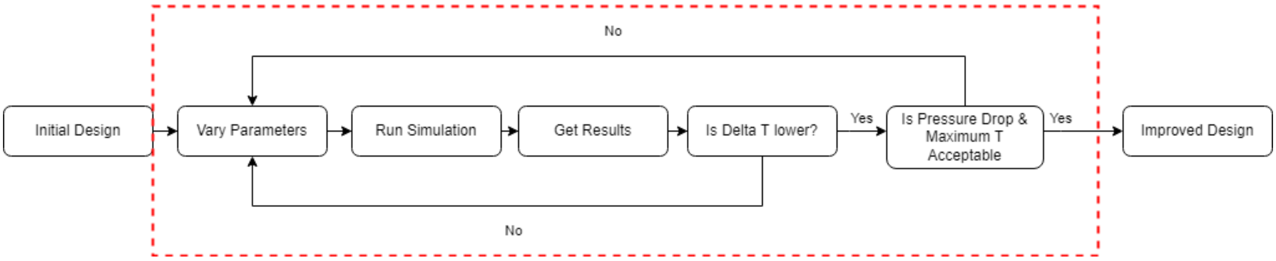

Figure 1.2: Basic flowchart of the workflow

1.4 Limitations:

The study will only consider the part of the BTMS that involves heat exchange between the coolant and the battery. A generic battery pack design will be used. The individual cells have the dimensions 50 mm x 90 mm x 190 mm and will be distributed in 4 rows, each containing 34 cells. Each battery cell will have a capacity of 150 Ah at 4.0 v. The maximum volume flow of the coolant is set to 40 l/min. The effect of different coolants, insulation and materials will not be investigated.

A simplification is made regarding how the batteries add heat to the system. Since simulations of the batteries' inner electrochemistry can become unnecessarily cumbersome the battery cells are regarded to be a volumetric heat source. The battery pack is assumed to add 5 kW of heat.

A simplification is also made regarding what happens to the energy after it has left the outlet. The rest of the BTMS is assumed to be able to deliver a constant coolant flow with a temperature of 287 K to the cooling plate inlet.

The methodology which will be the end product of this project should only aim to automatize the optimisation work of a simple geometry. Meaning that it is not meant to be applied to advanced geometries of many shapes and sizes. The methodology is mainly meant to show that it is possible to automatize the final stages of the optimisation work.

1.5 Ethical considerations

Lithium-ion batteries have a number of potential health and environmental risks associated with them. During the project these risks are considered when evaluating the cooling designs. For instance, the risk of thermal runaway is evaluated since thermal runaways are harmful to humans and the environment. Moreover, reducing the battery degradation leads to longer battery service lives, resulting in less natural resources being used.

In direct conjunction with how the project is executed no particular ethical considerations must be considered regarding the simulations. Ethical considerations regarding intellectual property, integrity and conflicts of interest are not an issue since the designs and configurations are our own ideas. In the development work we are fully transparent and honest irrespective if the results are positive or not.

2 Theory

In the theory chapter physical quantities and phenomena which affect the cooling configuration, the results and the credibility are presented and discussed. A brief description of the boundary layer and the theory behind the CFD simulations is also given.

2.1 Computational fluid dynamics

Computational fluid dynamics, or CFD for short, is a tool for solving fluid mechanics problems using computers. CFD can be used to solve problems regarding compressible or incompressible flow, turbulent or laminar flow. Using CFD, fluid behaviour, fluid interactions and heat exchange can be approximated [14]. CFD carries great advantages over experimental testing since the simulations do not require any expensive physical setups. CFD also allows for very large or very small systems to be simulated in very great detail. Worth noting is that a CFD simulation is only as good as the engineer who sets it up.

The first step to running a CFD simulation is pre-processing. Here the geometry is defined and every region and boundary must be well defined and contiguous. There can be no gaps in the geometry. The geometry is then discretized, discretization in the finite volume method (FVM) means that the domain is split into small finite volumes, for which the flow is solved [14]. The partial differential equations that govern the flow, conservation of mass and energy, are discretized into systems of algebraic equations which are solved at each of the finite volumes.

The small finite volumes make up the domain in a grid, often referred to as the mesh. Two examples of grids are staggered and collocated grids. In a collocated grid all parameters are calculated and stored at the central node in each cell volume. In a staggered grid, only the scalar values are stored in the central node and parameters like the velocity are stored at the cell face [15]. The grid can be structured or unstructured. Structured usually implies that the mesh is split into uniform rectangular elements. An unstructured mesh is made up of polyhedral or tetrahedral elements of different shapes and sizes.

The second step is modelling and discretizing the flow. To model the flow Navier-Stokes partial differential equations are used. Turbulent flows imply that there are chaotic, unpredictable and irregular terms in the turbulent part of the flow. The most common method of modelling turbulent flow is through the (time-averaged) Reynolds-averaged Navier Stokes (RANS) equations. By Reynolds-averaging the flow the turbulent terms become much more manageable for the computer. Two common turbulence models, $k-\epsilon$ and $k-\omega$, make use of the Boussinesq hypothesis for the Reynolds stresses. The two models are very similar, they solve two transport equations. One for the turbulent kinetic energy k and one for the dissipation of turbulent kinetic energy ϵ, or the specific dissipation of turbulent kinetic energy ω. The $k-\omega$ model is used when effects of the wall are of interest [14].

Differential equations have been discretized into algebraic expressions implying that one or more of the variables are dependent on one another. The solution must therefore be found iteratively. Both steady-state and transient problems can be solved. A transient solver takes more time but yields good results for both steady-state and transient problems. A steady solver on the other hand yields good results only for steady problems but takes a much shorter time [14].

2.2 Reynolds Number

The Reynolds number is a non-dimensional parameter that describes the viscous relation for Newtonian fluids and is calculated according to equation (2.1).

$$Re = \frac{VL}{\nu} \tag{2.1}$$

The parameters V and L describe the average velocity and the flows characteristic length scale respectively. The Reynolds number decides whether the flow is to be considered laminar or turbulent [16]. The Reynolds number is helpful in estimating the needed prism layer thickness in the boundary layer.

2.3 Boundary layer

In fluid flow, the region closest to the wall is called the boundary layer. It can be divided into three sub-layers, the Wall layer, Overlap layer and Outer layer. The Wall layer is located closest to the wall and is dominated by viscous shear stresses. In the Outer layer is the turbulent shear stress the most prominent. In the Overlap layer, which is located between the Wall layer and the Outer layer, both shear stresses are crucial [16].

$$u^* = \sqrt{\frac{\tau_w}{\rho}} \tag{2.2}$$

Equation (2.2) describes how the friction velocity, u^* depends on the density and the wall shear stress, τ_w in the Wall layer. The wall shear stress is calculated according to equation (2.3). Where f is the friction factor and V is the average velocity [16].

$$\tau_w = \frac{f \rho V^2}{2} \tag{2.3}$$

The friction factor for laminar flow in a circular pipe is obtained using equation (2.4) [16]. A circular pipe is the closest geometrical configuration to the rectangular duct used in this thesis. The laminar case is selected after checking the Reynolds number.

$$f_{lam} = \frac{64}{Re} \tag{2.4}$$

The velocity, u in the Overlap layer, is a logarithmic function of the distance to the wall, y, as well as the friction velocity and the kinematic viscosity accordingly to equation (2.5) [16]. The constants κ and B are set to 0.41 and 5 respectively.

$$\frac{u}{u^*} = \frac{1}{\kappa} \ln \frac{yu^*}{\nu} + B \tag{2.5}$$

A non-dimensional wall distance, y^+, is used to define where the sub-layers and their equations are valid. The Wall layer is situated from the wall up to $y^+ = 5$. The non-dimensional wall distance can be related to the real wall distance, y with the linear viscous equation (2.6).

$$u^+ = \frac{u}{u^*} = \frac{yu^*}{\nu} = y^+ \tag{2.6}$$

The Overlap layer starts at $y^+ = 30$ [16]. By using prism layers the entire laminar part of the boundary layer can be captured by ensuring that the first prism cell is located below $y^+ = 1$. It is important to capture the full boundary layer for the solution to be physical. There is a no-slip condition at the wall and the heat transfer occurs at the wall.

2.4 Thermodynamics

The rate of heat transfer is a function of the materials thermal conductivity, the temperature gradient and the contact area. The equation for heat flow is found from Fourier's Law, equation (2.7) [17]. Here q is the heat flux, k is the thermal conductivity, A is the surface area in contact and $\frac{dT}{dx_i}$ is the temperature gradient.

$$q_i = -k_i A \frac{dT}{dx_i} \tag{2.7}$$

Thermal contact resistance or thermal contact conductance is a measure of the ability to conduct heat between two bodies in contact, obtained by equation (2.8). Thermal contact conductance is the inverse of thermal contact resistance. The thermal contact resistance is mainly dependent on the surface roughness since the surface area in contact is what allows heat transfer to occur.

$$R_c = \frac{T}{qA} \tag{2.8}$$

By using a material with a higher thermal conductivity the heat can be exchanged more rapidly from the batteries to the coolant. Lowering the temperature of the coolant would also increase the rate of heat exchange since the temperature gradient will be greater. Increasing the contact area between the fluid and the cooling plate, i.e. increasing the cross-sectional area of the channels would also increase the rate of heat transfer.

Reducing the surface roughness would increase the area in contact between solids. The thermal contact resistance is thereby further reduced and consequently the heat transfer is increased. One way of circumventing the consideration of the surface roughness is to use a thermal interface material that can essentially fill all air pockets between the solids in contact.

2.4.1 Energy Balance

The law of conservation of energy states that energy can not be created or destroyed and a simple energy balance of the system is established in figure 2.1 and equation (2.9). Heat is added to the system by the battery cells in the form of a volumetric heat source. Energy is also added to the system by the coolant through the inlet, the change in kinetic and potential energy are negligible. Some energy exits the system through the boundary of the foam but most energy exits the system in the coolant through the outlet.

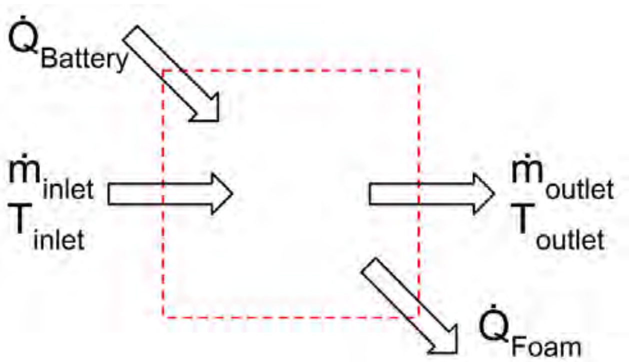

Figure 2.1: Simplified control volume of the cooling system

$$\begin{aligned}\dot{Q}_{Battery} + \dot{m}_{in} \cdot \left[c_p \cdot T_{in} + \tfrac{V_{in}^2}{2} + g \cdot z_{in}\right] = \dot{Q}_{Foam} + \dot{m}_{out} \cdot \left[c_p \cdot T_{out} + \tfrac{V_{out}^2}{2} + g \cdot z_{out}\right] \Rightarrow \cdots \\ \Rightarrow \dot{Q}_{Battery} - \dot{Q}_{Foam} = \dot{m} \cdot c_p \cdot (T_{out} - T_{in})\end{aligned} \tag{2.9}$$

2.5 Pressure drop

A pressure drop will occur when a fluid flows through a confined space, such as cooling channels. This is mainly due to friction. The pressure drop can be estimated using the Darcy-Weisbach equation (2.10). Where the pressure drop is expressed as a function of the friction factor, density, mean velocity, hydraulic diameter and the length of the channel. The friction factor is mainly dependent on the surface roughness of the channel walls [16].

$$\Delta p = f \cdot \frac{\rho}{2} \cdot \frac{V^2}{D} \cdot L \tag{2.10}$$

By making the channel longer or by decreasing the hydraulic diameter the flow is further restricted, increasing the pressure drop in the system. The mass flow rate has a great effect on the pressure drop since the pressure drop depends on the square of the average velocity in the channel.

2.6 Temperature variance

Due to natural variations in the manufacture of the batteries, a temperature variance will always be present in the battery pack. Since battery degradation is largely dependent on the temperature, the temperature variance should be minimized for all battery cells to have a similar life-span [10], [11]. Failure of individual cells leads to the battery pack performing worse, losing charging capacity and shortening its overall service life.

2.7 Battery modelling

The prismatic cell type is made up of layers of different materials and an electrolyte which leads to the battery cell having an anisotropic thermal conductance, equation (2.11). Along the span and length of the layers the thermal conductance is higher and perpendicular to the layers it is lower.

$$\begin{gathered} q_i = -k_i A \frac{dT}{dx_i} \\ k_x = 35 \; [W/mK], \quad k_y = 1 \; [W/mK], \quad k_z = 35 \; [W/mK] \end{gathered} \tag{2.11}$$

The heat generation of the battery pack, due to the internal resistance, is assumed to be 43000 $\left[W/m^3\right]$. The battery pack consists of 4 rows of 34 battery cells, each with a dimension of 50 mm, 90 mm and 190 mm which results in a total heat generation of $\approx 5000\ W$.

The battery cells are each enclosed in a thin sheet of aluminium to further improve the temperature distribution. The cells are also coated with an insulating foam against the rest of the battery pack, and between themselves. Between the battery shells and cooling plates there is no foam.

2.8 Battery thermal management system

The battery thermal management system (BTMS) is a key part of an electrical vehicle, its function is to protect the battery cells from experiencing large and sudden temperature changes. This is done by heating the battery when it is cold, cooling it when it is warm and insulating it from the ambient temperature conditions. Where the most important part is managing the temperature increase in the battery pack during charge and discharge [13]. Different systems are often categorized based on if the battery pack is cooled using air, liquid coolant or phase changing materials (PCM). Additionally the systems are separated on the basis if the cooling substance is in direct or indirect contact with the battery cells. Also whether the system is an active system and requires energy for the cooling or is a passive system and depends only on ambient conditions to cool the battery [13].

2.8.1 Air-cooled system

An air-cooled system uses air as its cooling medium. The main configurations are active and passive cooling. Usually air-cooled systems are open systems, meaning that air enters and exits the system as opposed to the closed loop configurations of the liquid-cooled system.

A passive configuration relies solely on heat dissipation to the ambience through the materials. This might work better during cruise where the dynamic air pressure supplies the system with colder air [18].

An active air-cooled configuration makes use of a fan to blow air on and around the battery cells. The air is usually taken from the ambience meaning that the cooling capacity of the air is limited by the ambient temperature. The air is then heated by the battery cells as it is forced through the battery pack and lastly the hot air exits the system and no further considerations must be taken for it [18].

An air-cooled system offers slightly worse cooling performance overall, as air has a lower heat capacity and lower thermal conductivity as opposed to its liquid-cooled counterparts. This leads to a higher temperature variance in the battery pack, leading to quicker battery degradation [19]. Because of this, air-cooled systems are much better suited for applications which offer slightly lower performance, and do not need as much cooling [19].

2.8.2 Liquid-cooled system

The simplest active liquid-cooled system requires a radiator, pump and coolant to function. More complex systems exist which include components such as secondary coolant loops, chillers, evaporators, compressors and condensers [13].

The higher efficiency of liquid-cooled systems leads to active air-cooled systems having a higher energy consumption compared to an active liquid-cooled system at equivalent cooling capacity [20]. Another advantage of an active liquid-cooled system is that it can also add heat to the battery pack, which improves the performance in cold climates. For these reasons active liquid-cooled cooling systems are the most widely used configuration in the industry today. However, liquid-cooled systems are more complex and consist of more components which makes them more expensive to develop and produce [20].

Direct liquid cooling has the potential to give better cooling performance due to no extra material being needed between the battery cells and the coolant which usually decreases the heat transfer. However direct liquid cooling systems are considered impractical because it requires a coolant that should have a large electrical resistance, be inflammable and dielectric for safety reasons. These types of coolants also have a higher viscosity than typical coolants which can be used in indirect cooling systems, resulting in larger energy consumption for an equivalent flow rate [20].

Thus indirect cooling is more widely used. Two typical designs used are cooling plates or discrete tubes, which are often combined with prismatic and cylindrical battery cells respectively. Discrete tubes are single channels which can be bent to follow the side of each battery cell. A cooling plate is a thin metal plate with internal channels for the coolant to flow through. It can be placed in three different configurations in relation to the battery pack. These are, between the battery cells, on one or several sides of the battery pack or internally placed micro-channels in the battery cells. There are two main types of channel designs, parallel and serpentine, depending on if the channels have bends inside the plate. Parallel channels do not have bends while serpentine channels do. The channel design and geometrical parameters can be optimised to maximize the cooling performance and minimise the pressure drop, resulting in enhanced efficiency [20].

2.8.3 PCM cooled system

Phase changing materials are materials that can absorb or emit a large amount of heat while changing from one physical state to another while keeping a constant temperature [21]. In comparison to liquid-cooled systems, PCM systems have the potential to be employed as passive cooling to lower battery temperatures during usage, reduce battery degradation due to a more even temperature distribution in the battery pack, and prevent thermal runaway. However PCM systems have some weaknesses, as low surface heat transfer coefficient, low thermal conductivity and the risk of running out of capacity to absorb heat [20].

To mitigate these drawbacks researchers have added different materials such as metal powder, foam, graphene, carbon fibre and carbon nanotubes to the PCM to create a composite with better thermal conductivity and surface heat transfer coefficient. Hybrid BTMS designs are also a method to transport heat from the PCM by combining it with air or liquid cooling. However more research in this area is needed to iron out these problems before a BTMS with PCM is usable in the industry [20].

3 Method

In the method chapter the geometries of the two designs and their differences are stated. The solver, models, mesh strategy and boundary conditions are also discussed. The aim of this study is for the results to be realistic, although some assumptions have to be made with regard to the solid mechanics of the materials. Since the strength of the materials will not be investigated, some qualified guesses and assumptions must be made to make sure that the design is still realizable. The chosen type of cooling system is an indirect liquid-cooled system, in accordance with the theory.

To automatize the work process the simulations were set up using Java script macros for Star-CCM+. Then a few parameters could easily be changed to generate a large number of simulations with small differences in the geometry and boundary conditions.

3.1 Geometry

The geometry for both cases consists of a battery pack containing 136 battery cells, an aluminium shell around each battery cell, isolation foam and one or multiple aluminium cooling plates. The dimensions of each battery cell are 50 mm x 90 mm x 190 mm, where 0.75 mm of the external part is a modelled aluminium shell. The inside of the battery cell is not modelled. The battery cells are placed in 4 rows with 34 cells in each column, spaced 3 mm apart in all directions, as shown in figure 3.1.

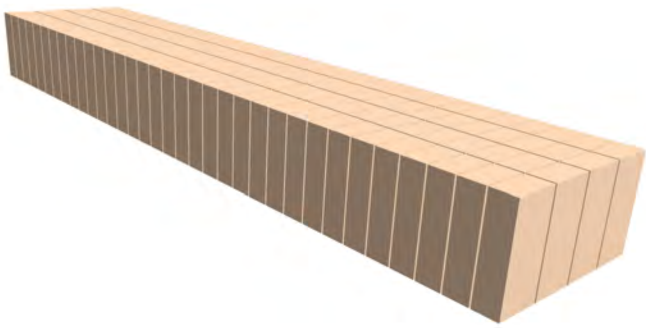

Figure 3.1: Battery pack iso-view

A 3 mm layer of isolation foam is placed around each battery cell to minimize the effect of the outside ambient conditions, as illustrated in figure 3.2 for the large cooling plate configuration. The foam is turned upside down in figure 3.2 to display the cutouts for the battery cells. The foam also lessens the effect of the surrounding battery cells on the individual cells, meaning that they contribute mainly to their own temperature increase rather than the other hot battery cells surrounding them. The foam will also take the pressure from bulging battery cells.

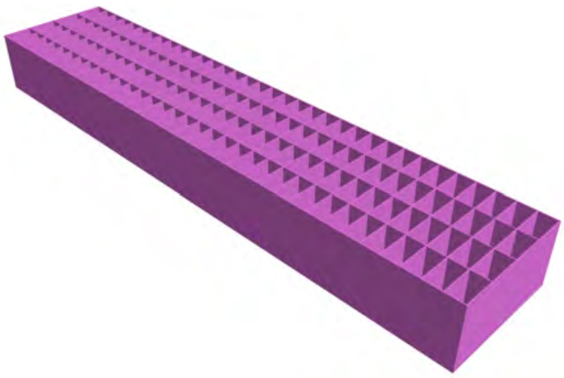

Figure 3.2: Isolation foam iso-view, upside down

A cooling plate consists of an aluminium plate with channels running through it. The thickness of the aluminium plate is 3 mm. The dimensions of the channel are to be varied in order to find an optimal design, although the height of the channel is restricted to 1 mm to ensure that structural rigidity can be assumed. For simplicity and realizability in fully parameterising the design for the Java script, the channels are built using rectangular blocks. The inlet and outlet are also required to be on the same side. This led to the decision to create channels of the "Triple U" design, containing four long straight channels connected by three U-turns, as shown in figure 3.3. The spacing between the long channels was set equal to the channel width to retain structure rigidity.

Figure 3.3: A cooling plate with one channel

For the cooling plate configuration where the battery pack is placed on top of a single large cooling plate the plate contains several sets of channels, as displayed in figure 3.4.

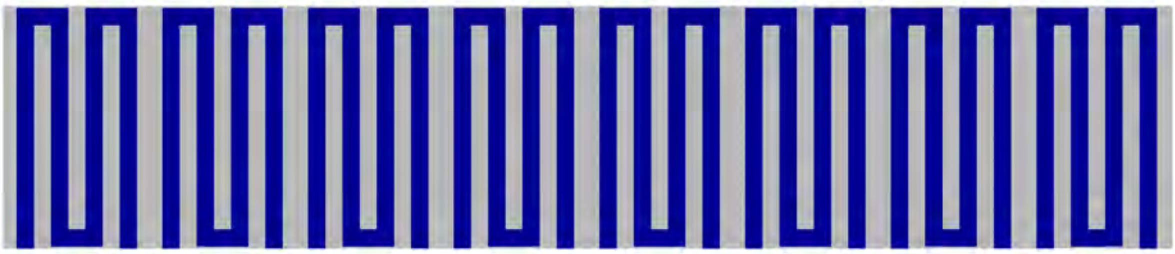

Figure 3.4: A cooling plate with several channels

3.1.1 Large cooling plate

The first design has only one cooling plate with the dimensions 375 mm x 1805 mm x 3 mm and is placed under the battery pack, as illustrated in figure 3.5. The cooling plate is as wide as 34 battery cells plus foam and it is as deep as four battery cells plus foam to cover the entirety of the battery pack. This is a common design used in the industry today due to the easy construction and maintenance.

Inside the cooling plate there are eight sets of "Triple U" channels, each with the dimensions 26.5 mm x 1 mm, as shown in figure 3.4. When changing the channel width the Java script was designed to insert as many sets of channels as the selected width would fit in the cooling plate. This was done in order to maximize the use of the plate and minimize the risk of battery pack sections not being cooled.

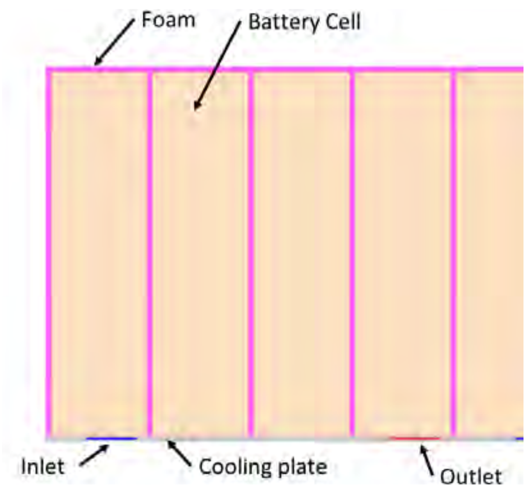

Figure 3.5: The large cooling plate configuration

3.1.2 Multiple cooling plates

For the second design 17 cooling plates are used, they are placed between every other column of battery cells on the short side of the battery pack, as illustrated in figure 3.6. The remaining gaps are filled with isolation foam. Each cooling plate contains one channel of the "Triple U" design, displayed in figure 3.3. The plates have a dimension of 375 mm x 3 mm x 190 mm, the plates are as high as the battery cells and as deep as four battery cells plus foam.

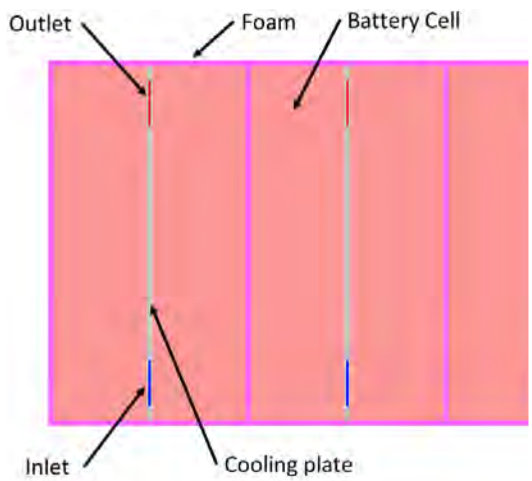

Figure 3.6: Multiple cooling plates configuration

3.1.3 Interfaces and contact resistance

To simulate the thin aluminium shells around the battery cells, shell regions were created based on the battery cell's external boundary. Automatically an interface between the battery region and the shell region is created.

Interfaces were established between the regions' boundaries to allow heat and energy transfer across different regions and materials. Two contact resistances were added to the interface between the cooling plate and the battery shells, as well as the battery shell and the battery cell, to simulate the thermal contact resistances of the heat transfer, mainly caused by different surface roughnesses. The contact resistance is high between the battery cell and its shell since they have less contact. The contact resistance is lower between the shell and cooling plate since both are made of aluminium and are held in contact by the battery pack.

In the interfaces containing coolant or foam the contact resistance was assumed to be zero, due to the assumption that the liquid and foam will fill any air pockets created by the surface roughness, yielding a perfect thermal contact conductance. All interfaces and their contact resistances are displayed in table 3.1.

Table 3.1: Contact resistances of the boundary interfaces

Interface	**Contact resistance** $[m^2 \cdot K/W]$
Coolant: Boundary - Cooling plate: Boundary	0
Plate: Boundary - Foam: Inside & Bottom Boundary	0
Plate: Boundary - Battery Shell: Outside Boundary	5E-4
Battery Shell: Outside Boundary - Foam: Inside & Bottom Boundary	0
Battery Shell: Inside Boundary - Battery cells: Boundary	0.01

3.2 Models and materials

Physics continua were created to model the different materials, one for the coolant, the aluminium cooling plate, the aluminium shell and the battery cells. The selected models for the solid regions are presented in table 3.2. For the battery cells, the foam and the aluminium plate the same solid models were used, three-dimensional steady-state segregated solid-energy. For the aluminium shell the Shell Three Dimensional model was used, this was done to model the shells rather than having to mesh them using an automated mesh operation, since they are very thin. The battery shells were meshed as a 2D approximation to represent a thin volume mesh. Segregated Solid Energy was used to model the heat transfer within and between the different parts.

Table 3.2: Solid models

Battery cell, Plate, Foam	**Shells**
Constant Density	Constant Density
Gradients	Gradients
Segregated Solid Energy	Segregated Solid Energy
Solid	Solid
Solution Interpolation	Solution Interpolation
Steady	Steady
Three Dimensional	Shell Three Dimensional

The models used for the liquid coolant are presented in table 3.3. K-Omega Turbulence model was chosen to model the turbulent flow and capture its wall effects. The wall effect means that the average velocity of the flow is proportional to the logarithm of the wall distance, as described in the Boundary Layer theory section 2.3. The segregated solvers are used since they require less computing power and speed up the solution. The segregated solvers can be used since the mach numbers are relatively low and the density is constant.

Table 3.3: Liquid models

Coolant
All y+ Wall Treatment
Constant Density
Gradients
K-Omega Turbulence
Liquid
Reynolds-Averaged Navier-Stokes
Segregated Flow
Segregated Fluid Temperature
Solution Interpolation
SST (Menter) K-Omega
Steady
Three Dimensional
Turbulent
Wall Distance

The material properties of the regions are presented in table 3.4. The battery cells have an anisotropic thermal conductivity due to the stacking of inner material sheets. Along the shortest side, perpendicular to the inner material sheets, the thermal conductivity is 1 $W/(m \cdot K)$ and in the other two directions the thermal conductivity is 35 $W/(m \cdot K)$. The coolant consists of ethylene glycol, the shells and plate are made of aluminium and the foam is a generic isolation foam.

Table 3.4: Material properties

Properties	**Battery**	**Shells and Plate**	**Coolant**	**Foam**
Density $[kg/m^3]$	2300	2702	1070	1000
Specific Heat $[J/(kg \cdot K)]$	1200	903	3400	350
Dynamic Viscosity $[Pa \cdot s]$	-	-	0.005	-
Thermal Conductivity $[W/(m \cdot K)]$	Anisotropic k_{11}: 35 k_{22}: 1 k_{33}: 35	237	0.4	0.03

3.3 Mesh

The surface remesher and the polyhedral mesher was used for all four continua regions. The surface remesher divides the surfaces into small enough cells to make sure that the mesh is conformal and to improve the surface quality. The polyhedral mesher was used because it is the recommended core mesh for internal flows. A triangular mesher usually suffices for solid regions, but to ensure conformal mesh connections between the liquid and solid regions, polyhedral meshes were also used for the solid regions. The selected meshers used in each region are presented in table 3.5.

Table 3.5: Meshers for the solid and liquid regions

Battery, Plate, Foam	**Coolant**
Surface Remesher Polyhedral Mesher	Surface Remesher Polyhedral Mesher Thin Mesher Prism Layer Mesher

In the coolant region the Thin Mesher was used to make sure a sufficient number of cells were present in the height of the channels, despite the small height of 1 mm. A cross-section of the mesh in the height direction is displayed in figure 3.7. The Prism Layer Mesher was used to capture the boundary layer along the channel walls. The coolant mesh was set up as a uniform mesh, where the target surface size is 100 % of the base size, as is shown in figure 3.8.

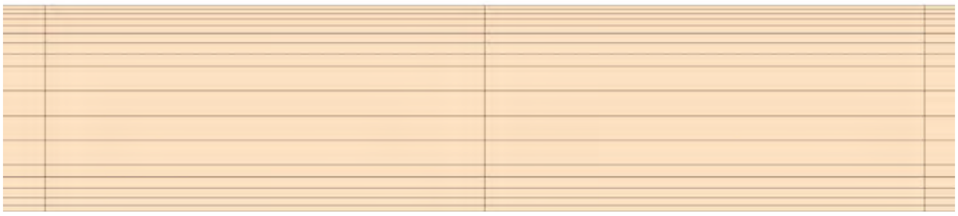

Figure 3.7: coolant mesh, showing thin layer and prism layer

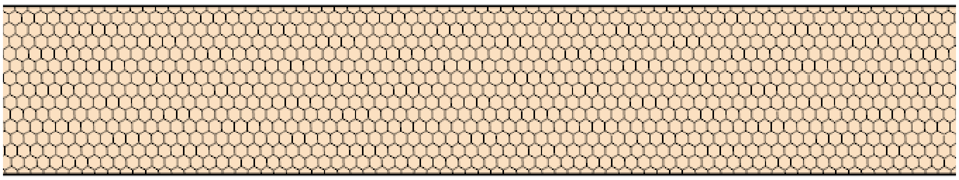

Figure 3.8: coolant mesh, showing polyhedral elements

The Base Sizes of the regions were changed in the default mesh controls to get a small enough cell size to capture the flow and heat transfer gradients within and between the different regions. The number of thin layers was set to six to generate a mesh with a smooth cell size transition between the Prism layer and the core mesh in the height direction. Along the channel width, smooth cell size transitions were achieved by using small enough cell sizes throughout the whole domain. The base sizes and the number of thin layers are presented in table 3.6.

Table 3.6: Default mesh controls

Setting	**Battery**	**Plate**	**Foam**	**Coolant**
Base Size [m]	0.01	0.03	0.04	0.02
Number of Thin Layers	-	-	-	6

Due to the wide and flat geometry of the channels, different prism layer settings were needed in the vertical and horizontal directions. Surface Controls were created, one for the sides of the channel and one for the top and bottom of the channels. Using a surface control the mesh settings can be overwritten in the selected surfaces' normal direction.

Using equations (2.1)-(2.6) the required first prism cell height for y^+ to be less than 1 was calculated. By choosing an appropriate number of prism layers and prism layer stretching the total thickness of the prism layers was calculated and is shown in table 3.7.

Table 3.7: Mesh surface controls

Setting	**Coolant: Top and Bottom**	**Coolant: Sides**
Number of Prism Layers	7	10
Prism Layer Stretching	1.2	1.2
Prism Layer Total Thickness [m]	2.2162497926596933E-4	8.076789539759221E-4

3.4 Boundary conditions

The total amount of heat generated by the battery pack is assumed to be 5000 W, which results in a volumetric heat source of roughly 43000 W/m^3 since the total battery volume is 0.11628 m^3. The volume flow of the coolant is assumed to be 40 l/min at a temperature of 287 K. This yields a coolant mass flow of roughly 0.713 kg/s, taking the density into account. The outer boundary of the foam is assumed to not be perfectly adiabatic and therefore a slight heat flux of 10 W/m^2 is applied. All boundary conditions for the regions' boundaries are shown in table 3.8.

Table 3.8: Boundary conditions for all regions

Region/ Boundary	**Boundary condition**	**Values**
Battery	Wall	Volumetric Heat Source: 43000 W/m^3
Channels Inlet	Mass flow Inlet	Mass flow: 0.713 kg/s, Temperature: 287 K
Channels Outlet	Outlet	-
Channels Walls	Wall	-
Foam (Outer boundary)	Wall	Heat Flux: -10 W/m^2
Foam	Wall	-
Shells	-	-
Plate	Wall	-

3.5 Post-Processing

The results should be evaluated in terms of pressure drop, overall cooling capabilities and the uniformity of the cooling. The pressure drop of the system is found as the pressure difference at the inlet and the outlet. The pressure is monitored and surface-averaged at the inlet and outlet to ensure a uniform pressure distribution and get an accurate pressure reading.

The average battery cell temperature was evaluated as the volume-averaged temperature of the cell. Monitoring the average temperature of each battery cell makes it possible to find both the maximum battery cell temperature in the battery pack and also the maximum temperature difference of all battery cells. The volume-averaged temperature is also representative of the whole cell since the battery cell is modelled as a volumetric heat source with an anisotropic thermal conductivity.

It is also important to check that the residuals in the solution converge. The default residuals defined by Star-CCM+ are the momentum equations, energy equation, turbulent kinetic energy and turbulent dissipation rate. A user defined residual was also created, it monitors the total heat flux into and out of the system. This residual should be close to zero for a converged solution. The solution should also be mesh independent and therefore a mesh independence study is also conducted.

3.6 Automatic Optimisation

As a means to automatize the optimisation, a Star-Java macro which allows for parameterization of the geometry, creation of the geometry, meshing and simulation will be developed. All necessary metrics for evaluation of the performance will be outputted from the script for minimum user input necessity. The most significant performance metrics are, in descending order, maximum battery cell temperature difference, maximum battery cell temperature and lastly pressure drop.

As explained in the flowchart of operations in figure 1.2 in the introduction, the initial design will be varied and the script will be run until a minimum battery cell temperature difference is found. The parameter that was chosen for the optimisation was the channel width, which is the main mean of varying the interface area of the fluid and the cooling plate. The mass flow rate which has a large effect on the pressure drop will also be varied.

3.7 Transient simulations

To further evaluate the performance of the better cooling system configuration, a transient simulation will be run. This is done to investigate the time dependencies. For instance, finding out how long it takes for the batteries to reach their maximum temperature and how long it takes for the cooling system to cool the batteries at full capacity.

The transient simulation is set up as implicit unsteady and uses a temporal (time) discretization of the 1st-order. The transient simulation will be run using varying time scales since the flow is easier to solve than the energy balance. The energy transfer takes longer to converge than the segregated flow solution.

3.8 Further Processing of Multiple Plates Configuration

Using the results from the optimisation work, further processed designs based on the observed trends are developed. Only the multiple cooling plates configuration is processed further. Since the cooling plates are placed between the battery cells and not under the relatively heavy battery pack, like for the large cooling plate configuration, the approximated requirements for structural rigidity were toned down.

3.8.1 Wider Triple U design

Since the Triple U design proved to be efficient at cooling the battery pack it was investigated if it could be improved by widening the channels, from 26.5 mm to 41.25 mm, as illustrated in figure 3.9.

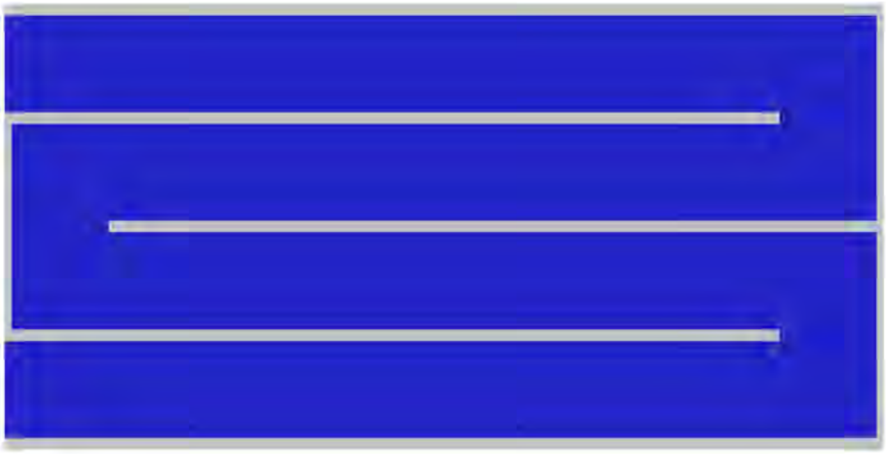

Figure 3.9: Wider Triple U channel

3.8.2 Wider Triple U design With Fins

Fins were added to the Wider Triple U design to increase the surface area. The fins are each 41.25 mm long and 1 mm wide and were added in the middle of the channels, as shown in figure 3.10.

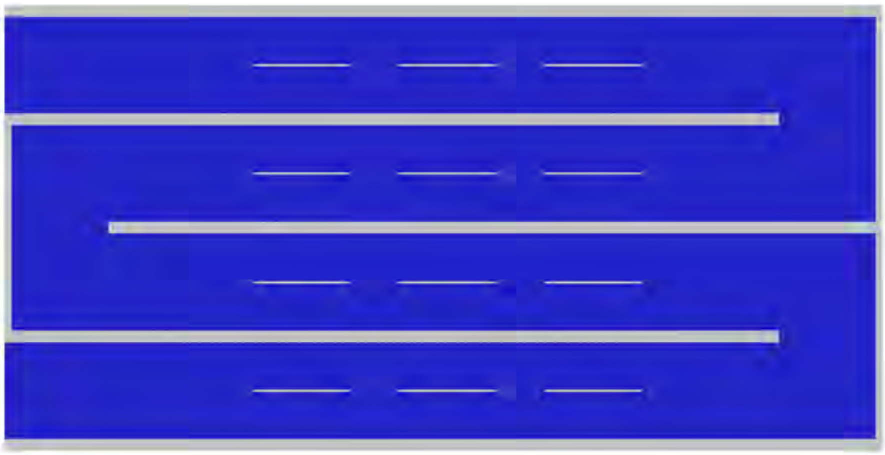

Figure 3.10: Wider Triple U channel with fins

3.8.3 Five U design

A Five U design consisting of six straight channels connected by five U-turns was constructed, as displayed in figure 3.11. This design has the same channel width as the original triple U design, 26.5 mm, but thinner aluminium walls to make room for five U-turns.

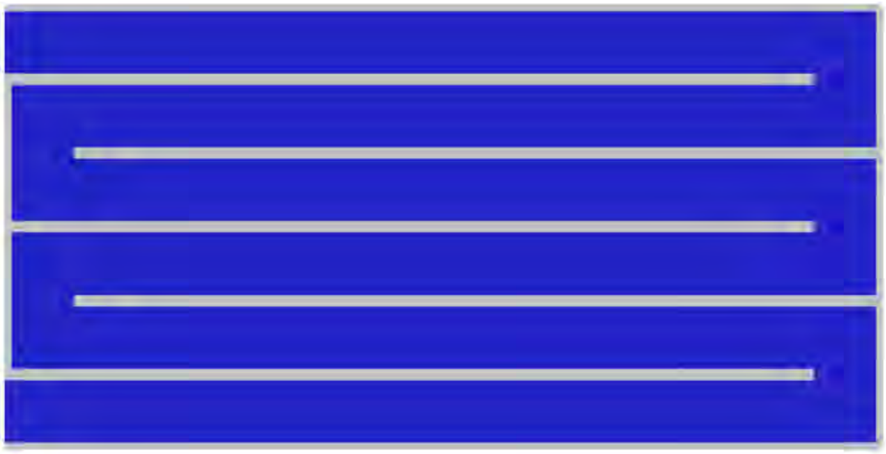

Figure 3.11: Five U channel design

3.8.4 Single U Channel

A Single U channel design with five inner channels was created, as illustrated in figure 3.12. The innermost channel is 8 mm wide and the channel width increases by 20 % from channel to channel.

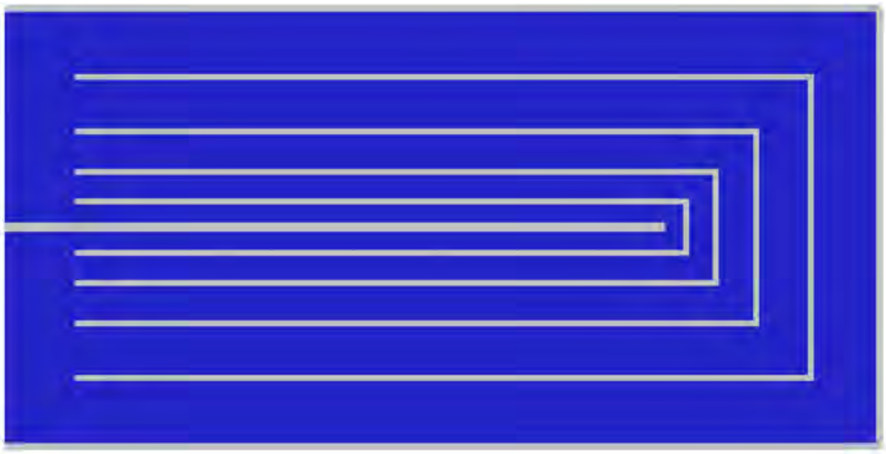

Figure 3.12: Single U channel design

4 Result

In this section, the results from the CFD simulations are presented. First the results for the two cooling plate configurations, large cooling plate and multiple cooling plates, are presented. Followed by the results for the four continuation designs of the multiple plate configuration. Results from the transient simulations, varied inlet temperature and changed battery anisotropic thermal conductivity using the multiple plate design are also presented. Lastly, a mesh convergence study was conducted for each of the designs to ensure that the solutions are independent of the mesh.

4.1 Large cooling plate

The result for the large cooling plate design for all channel widths is presented in figure 4.1 and table 4.1. The volume averaged temperature difference and pressure drop is plotted against the channel width in figure 4.1a and 4.1b respectively. A large cooling plate with a channel width of 10 mm resulted in the lowest maximum battery cell temperature of 326.7 K and the lowest minimum temperature of 325.9 K. Resulting in a temperature difference of 0.855 K. The 10 mm channel width design also yielded the largest interface area of 0.7318 m^2.

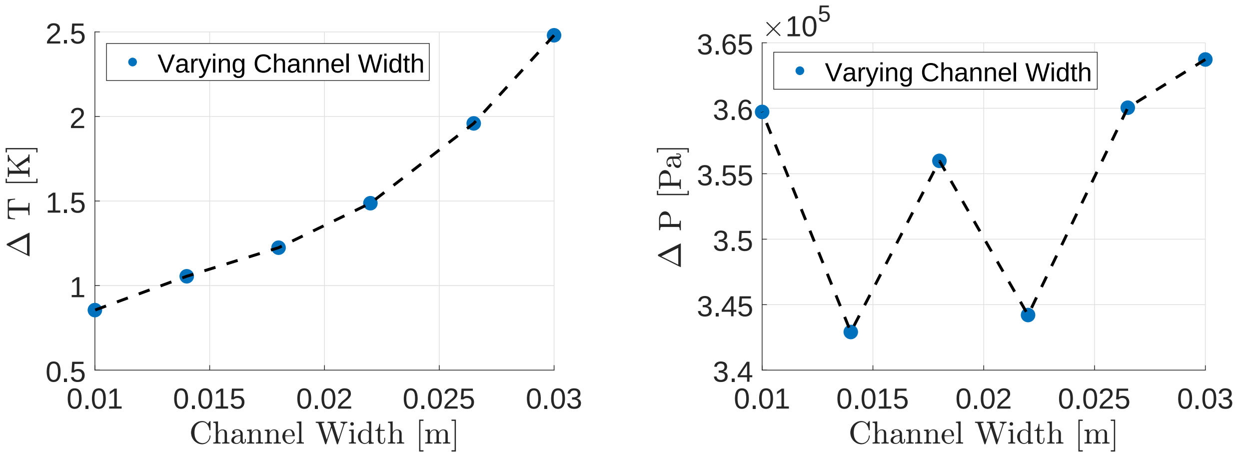

(a) Temperature difference versus channel width

(b) Pressure drop versus channel width

Figure 4.1: Temperature difference & Pressure drop plots for the large cooling plate

The varying channel widths yielded similar pressure drops, as shown in table 4.1. The lowest pressure drop, 342 912 Pa, was achieved by the design with a channel width of 14 mm. The 30 mm channel width design resulted in the highest pressure drop, temperature difference, maximum and minimum temperatures for the battery cells. It also has the lowest interface area among the various channel width designs.

Table 4.1: Large cooling plate result, varying channel width

Width [mm]	**Area [m^2]**	**ΔP [Pa]**	**ΔT [K]**	**Min T [K]**	**Max T [K]**
30	0.6822	363 725	2.480	326.432	328.912
26.5	0.6871	360 043	1.959	326.327	328.286
22.0	0.7121	344 209	1.487	326.230	327.717
18.0	0.7004	355 984	1.224	326.123	327.347
14.0	0.7315	342 912	1.055	325.863	326.918
10.0	0.7318	359 721	0.855	325.863	326.718

4.2 Multiple cooling plates

The channel dimension which yielded the lowest temperature difference, lowest pressure drop and lowest maximum temperature, was a channel width of 26.5 mm, as shown in figure 4.2a, 4.2b and table 4.2. This design yielded the largest interface area of 1.46 m^2. The maximum battery cell temperature for the 26.5 mm channel width was 305.3 K and the minimum temperature was 304.9 K. Resulting in a temperature difference of 0.403 K.

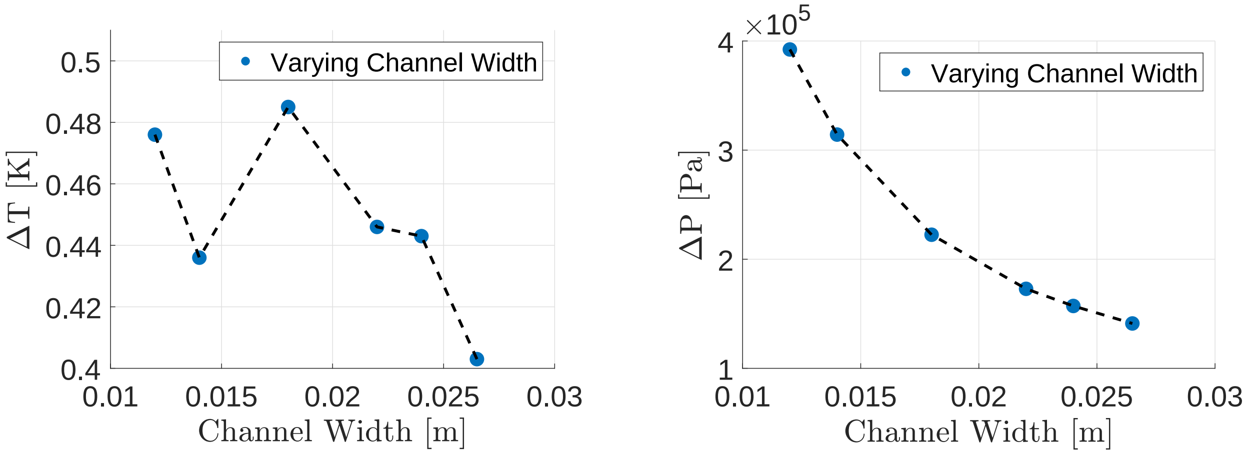

(a) Temperature difference versus channel width

(b) Pressure drop versus channel width

Figure 4.2: Temperature difference & pressure drop plots for varying channel widths

The pressure drop decreased with an increasing channel width as shown in table 4.2. The 12.0 mm channel width design yields a pressure drop of 392 245 Pa and the 26.5 mm channel width design yields a pressure drop of 141 129 Pa.

Table 4.2: Multiple plates result, varying channel width

Width [mm]	**Area** [m^2]	Q **[l/min]**	**ΔP [Pa]**	**ΔT [K]**	**Min T [K]**	**Max T [K]**
26.5	1.460	40	141 129	0.403	304.912	305.315
24.0	1.321	40	157 172	0.443	305.233	305.676
22.0	1.211	40	172 884	0.446	305.595	306.041
18.0	0.992	40	222 458	0.485	306.191	306.676
14.0	0.777	40	314 231	0.436	307.484	307.919
12.0	0.671	40	392 245	0.476	308.240	308.716

The 26.5 mm design was run for varying volume flow rates. For a volume flow rate of 40 l/min the pressure drop was found to be 141 129 Pa. Lowering the volume flow decreased the pressure drop and increased the temperature difference, as shown in figure 4.3a and 4.3b.

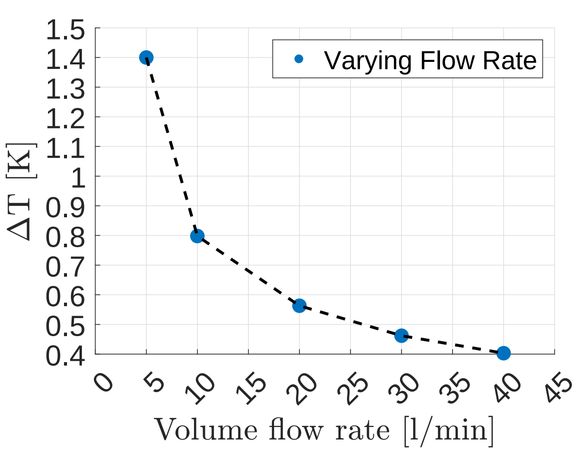

(a) Temperature difference versus volume flow rate

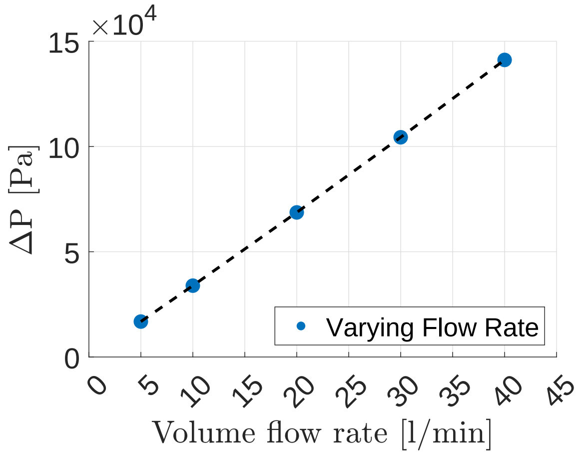

(b) Pressure drop versus volume flow rate

Figure 4.3: Temperature difference & pressure drop plots for varying flow rates

Decreasing the volume flow rate also increased the maximum temperature as shown in table 4.3. At 40 l/min the maximum battery cell temperature was 305.3 K and at 5 l/min the maximum battery cell temperature was 313.9 K.

Table 4.3: Multiple plates result, varying volume flow rate

Width [mm]	**Area [m^2]**	Q **[l/min]**	**ΔP [Pa]**	**ΔT [K]**	**Min T [K]**	**Max T [K]**
26.5	1.460	40	141 129	0.403	304.912	305.315
26.5	1.460	30	104 387	0.462	305.341	305.803
26.5	1.460	20	68 683	0.563	306.155	306.718
26.5	1.460	10	33 889	0.798	309.384	308.586
26.5	1.460	5	16 825	1.400	315.273	313.873

4.3 Processing of the Multiple Plates Configuration

The further processed designs of the multiple plate configuration yielded mixed pressure drops and temperature differences for a coolant flow of 40 l/min, as presented in table 4.4. The design consisting of 5 U channels had the lowest temperature difference of 0.337 K and the lowest maximum temperature of 304.7 K. This design also resulted in the highest pressure drop 206 010 Pa. The Single U channel design resulted in the highest temperature difference, 0.726 K and the lowest pressure drop 22 135 Pa but it had the largest interface area of 2.175 m^2.

Table 4.4: Results from processing of the multiple plates configuration

Design	**Area** $[m^2]$	**ΔP [Pa]**	**ΔT [K]**	**Min [K]**	**Max T [K]**
Triple U	1.460	141 129	0.403	304.912	305.315
Wider Triple U	2.150	83 461	0.529	304.346	304.875
Wider Triple U & Fins	2.151	85 399	0.516	304.310	304.826
Single U Channel	2.175	22 135	0.726	304.318	305.044
Five U	2.099	206 010	0.337	304.343	304.681

The designs were run for multiple decreasing mass flow rates to yield results for varying pressure drops. The volume flow rates varied from 5-40 l/min for every design. The subsequent pressure drops are plotted together with the maximum battery cell temperature in figure 4.4a and temperature difference in figure 4.4b. The highest flow rate corresponds to the highest pressure drop and vice versa for each design.

The Single U design yielded a maximum temperature ranging from 305-310 K at a pressure drop ranging from 22-5 kPa. At the same pressure drops the temperature difference ranged from 0.726-1.890 K. The Single U design therefore generates a higher temperature difference generally compared to the other designs. The performance is generally equivalent between the Wider Triple U design and the Wider Triple U design with fins. There is a slight difference at the maximum flow rate, i.e. at the highest pressure drop, where the Wider Triple U with fins design shows a lower temperature difference. The original Triple U and the Five U designs gave the highest pressure drops for all maximum temperatures compared to the other designs. The Five U design gives the lowest temperature difference of all the designs but at a high pressure drop.

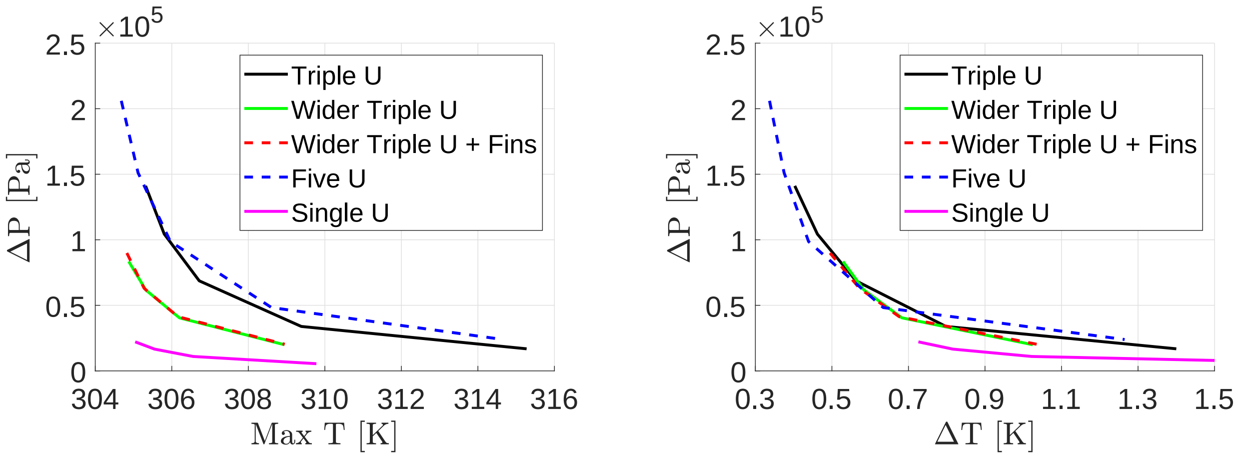

(a) Pressure drop versus maximum temperature

(b) Pressure drop versus temperature difference

Figure 4.4: Results for varying volume flow rates

4.4 Increasing Inlet Temperatures

The 26.5 mm Triple U design with a volume flow of 40 l/min was run for multiple inlet temperatures to investigate the inlet temperature's effect on the maximum battery cell temperature and temperature difference. The maximum average battery cell temperature turned out to be linearly dependent on the inlet temperature while the temperature difference was not affected at all, as is shown in figure 4.5a and 4.5b. The pressure drop is also unaffected since the small change in temperature has no effect on the flow. For an inlet temperature of 290 K the maximum temperature of all battery cells is ≈ 308.15 K, i.e. for all battery cells to operate within the optimal range of temperatures the inlet temperature should not exceed 290 K for the original Triple U design.

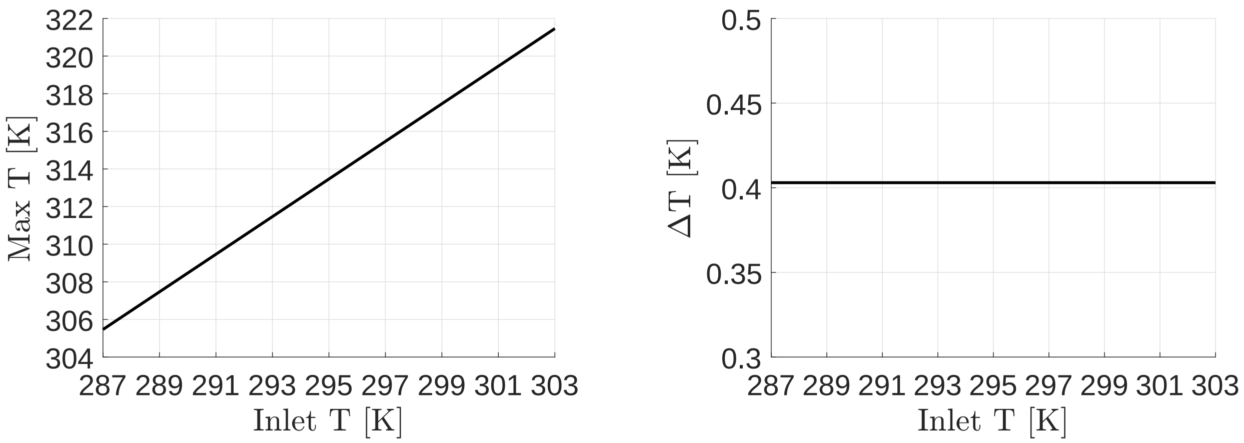

(a) Maximum temperature versus inlet temperature

(b) Temperature difference versus inlet temperature

Figure 4.5: Varying inlet temperature for Triple U

4.5 Changing the anisotropic thermal conductivity of the battery cells

The anisotropic thermal conductivity was changed to see if the current battery design could be altered to better match the multiple cooling plate configuration. The thermal conductivity was rotated 90 ° by modifying k_{11} to 1 $W/(m \cdot K)$ and k_{22} to 35 $W/(m \cdot K)$. This means the direction with low thermal conductivity was no longer situated in the normal direction of the cooling plates. The original Triple U design with a channel width of 26.5 mm and volume flow of 40 l/min was used in the simulation, resulting in a maximum volume average temperature of 302.8 K and a temperature difference of 0.323 K.

4.6 Transient simulations

For the transient simulations, three cases were chosen arbitrarily to investigate the performance of the cooling system. The design used was the original Triple U design.

4.6.1 Maximum power output, maximum battery strain

Starting all battery cells at 287 K, with the cooling system at full power, i.e. a flow rate of 40 l/min, it takes roughly 1 hour of physical time for the battery cells to reach their maximum volume average temperature. Each battery cells temperature is plotted against the physical time in figure 4.6. The maximum temperature reaches 305.3 K and the temperature difference reaches 0.399 K. The unsteady solution therefore corresponds to the steady solution.

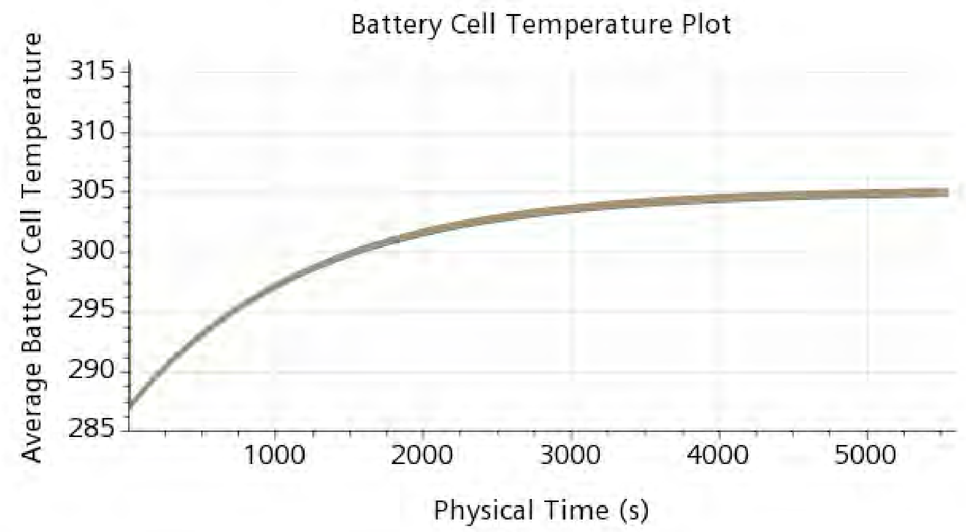

Figure 4.6: Battery cell temperature plot, heating from cold

4.6.2 Halved power output

Running off the previous case, the power output from the battery pack is cut in half. The cooling system is still running at 40 l/min. It takes approximately 4000 seconds for the volume average temperature of the battery cells to drop to $\approx 296K$, as shown in figure 4.7. The temperature difference is 0.301 K and the maximum average temperature of any battery cell is 296.3 K.

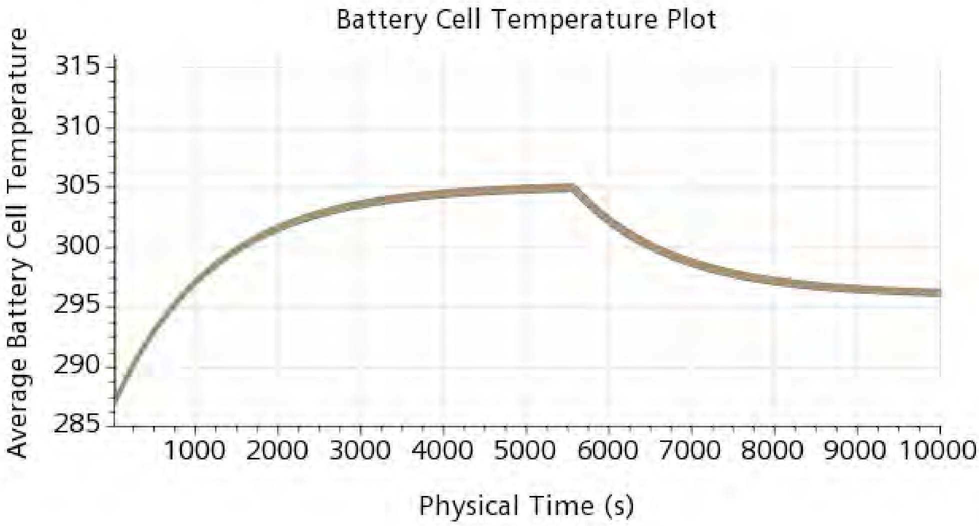

Figure 4.7: Battery cell temperature plot, halving power output

4.6.3 Crisis simulation, critical temperature

In the third case, displayed in figure 4.8, the cooling system is completely shut off until all battery cells exceed the critical temperature of 60 $°C$ to evaluate if the cooling system can handle critical temperatures in the battery pack. Running the battery pack at full power with no cooling it takes $\approx$ 4100 seconds for all battery cells to reach a critical temperature. The flow rate is then set to 40 l/min and it takes $\approx$ 2400 seconds for all battery cells to cool within the optimal range of 15-35 °C, while still running the battery pack at full power.

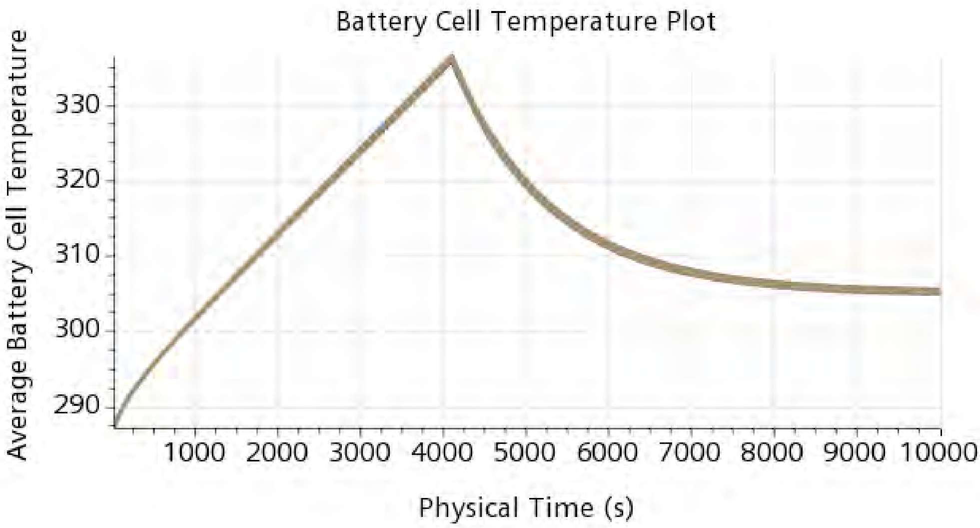

Figure 4.8: Battery cell temperature plot, crisis simulation

4.7 Mesh Independence Study

A mesh study was carried out for both cooling plate configurations and for each new multiple cooling plate design. The aim of the mesh studies is to ensure that the results are mesh independent. Only the base size of the coolant was varied during this mesh study. For the solid parts, Foam and Plate, a separate mesh study was conducted. The Battery cells were always meshed using a base size of 0.01 m, which was deemed a fine mesh after visual inspections and only added up to approximately 150 000 cells. The pressure drop and the maximum volume average battery cell temperature were deemed to be the most suitable parameters to compare in the mesh study. A corresponding pressure drop between different meshes assures that the flow is captured correctly and corresponding maximum temperatures guarantee that the heat transfer solution within the coolant and between the adjacent regions is mesh independent.

For the solid region mesh study, a fine coolant mesh with a base size of 0.01 m was used to ensure minimal error influence from the coolant mesh. The original Triple U multiple plate design was used in the solid mesh study. In the mesh study for the solid regions, only the maximum temperature was of interest due to the solid region mesh only affecting the heat transfer between the battery pack and coolant. The solid region mesh is considered converged at a base size of 0.04 m since it yields the same results as the finer solid region meshes, as shown in table A.1. Coarsening of the mesh will however affect the solution negatively since the maximum temperature starts to deviate.

The results from the coolant mesh studies are presented in tables A.2 - A.6 in appendix. The pressure drop changes less than 0.2% as the base size is decreased, and the number of cells is increased. The maximum temperature also varies less than 0.2%, suggesting that the solutions using base size 0.02 m are all mesh independent. The design Wider Triple U with fins was excluded from the mesh study due to the small difference in geometry and results compared to the Wider Triple U design, see table 4.4.

Since the capture of the boundary layer is dependent on the solution's ability to capture $y^+ < 1$, the condition for $y^+ < 1$ was evaluated for the mesh independent solutions. Plots of y^+ for all designs are illustrated in figures B.1-B.6 in appendix. The large cooling plate was the only design which had some small regions with $y^+ > 1$, all other designs had $y^+ < 1$ in the entire coolant region. This does not lead to any issues however, since the only region where $y^+ > 1$ occurred was on the inside of the bend of the U-turns where there are high velocities locally.

5 Discussion

In the discussion section the two cooling configurations are first evaluated and compared. Then the processed multiple plate designs are compared to each other and the original Triple U design. The weaknesses and strengths of each design are highlighted. Then a general discussion is made about which of the designs is best. Lastly a discussion is made regarding the realizability of the design and if the simulations are realistic and some limitations of the study.

5.1 Comparing the two cooling configurations

The cooling performance of the large cooling plate is poor compared to the Triple U multiple plate design. Both when analyzing the maximum temperature and the temperature difference for varying channel widths in the tables 4.1 and 4.2. Between the large cooling plate and multiple cooling plate configurations, the maximum temperatures for the best designs differ by 21.4 K. For the best large cooling plate design, the temperature difference is 0.452 K higher than the best multiple plate design. This is illustrated in figure 5.1 where the temperature of all battery cells is plotted for a converged steady-state solution. The multiple cooling plates configuration has a lower maximum temperature and lower point temperature difference.

The coldest large cooling plate design has a maximum temperature of 326.7 K, which corresponds to 53.6 °C. Such high temperatures would result in substantial wear of the battery pack and a high risk of thermal runaway occurring, according to the theory. For the coldest Triple U multiple plate design the maximum temperature was 305.3 K, which equals 32.2 °C. At this temperature there is no risk of thermal runaway occurring or accelerated battery degradation. A trend observed in the result tables 4.1 and 4.2 is that increasing the interface area yielded lower maximum temperatures and lower temperature differences between the battery cells, i.e improved cooling performance.

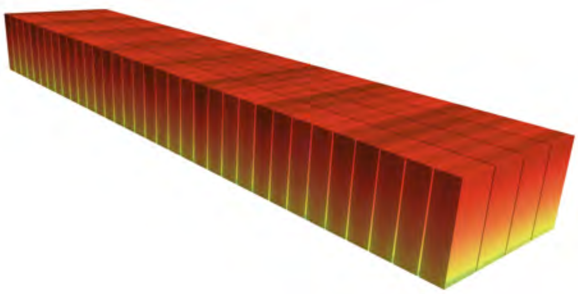

(a) Large cooling plate configuration

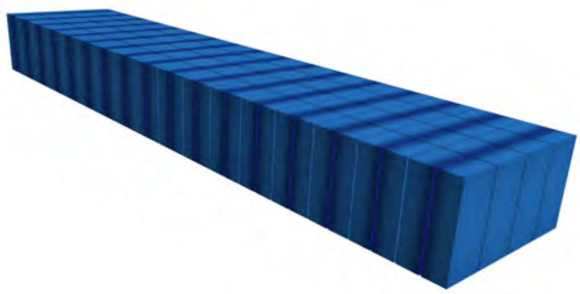

(b) Multiple cooling plates configuration

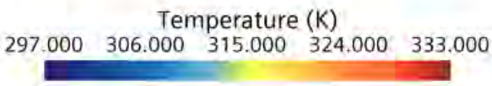

Figure 5.1: Temperature plots of the battery pack

There are several explanations for the large cooling plate configuration performing worse. The best multiple plate design has a considerably larger interface area than the best large plate design. However the multiple cooling plate design with 12 mm wide channels has a comparable interface area to the large cooling plate design with 30 mm wide channels. Still there are large differences in the maximum temperature and temperature difference between the two configurations. This is due to the positioning of the plates, cooling the battery pack with only one side of the plate results in the interface area being used less effectively. The boundary heat flux between the coolant and the plate is plotted for both sides of the large cooling plate and for one side of the multiple plate design in figure 5.2. The plots in figures 5.2a and 5.2b are zoomed in on a single channel in the large cooling plate. The top side, which is facing the battery pack, has a higher heat flux. Meaning that more heat is transported through the top side, than through the bottom side. Due to the simulations being run in steady state, low heat flux is expected for a good cooling performance, since heat flux depends on the temperature difference, according to equation (2.7). The heat flux of the multiple plate design is lower compared to the top side of the large plate, as is shown in figure 5.2c and 5.2a. Suggesting that the plate and coolant temperatures are closer for the multiple plate design, which is the result of a battery pack with lower temperature.

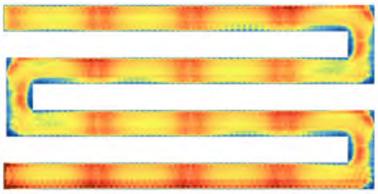

(a) Top side

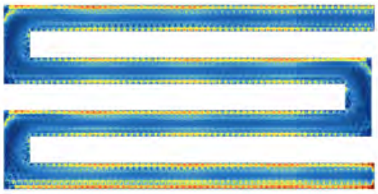

(b) Bottom side

(c) Multiple cooling plates

Figure 5.2: Boundary heat flux plots, large cooling plate & multiple cooling plates

Surface temperature plots at the surface of the aluminium plates of the two configurations are compared in figure 5.3. The large cooling plate's surface temperature, shown in figure 5.3a, is zoomed on one part of the plate covering a single channel. The multiple cooling plate configuration, shown in figure 5.3b, results in a cooling plate with generally a lower temperature than the large cooling plate. The maximum temperature is also higher for the large cooling plate configuration. The large cooling plate was dropped from any further optimisation work due to the large differences in cooling performance between the configurations.

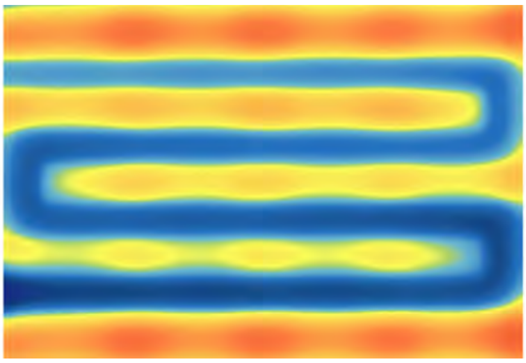

(a) Large cooling plate

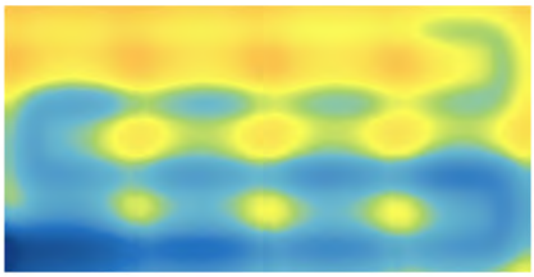

(b) Multiple cooling plate

Figure 5.3: Temperature plot of the cooling plate surface.

For the multiple plate design the pressure drop increased when the channel width was decreased, as shown in table 4.2. Making the channels narrower decreased the cross-sectional area, forcing the velocity to increase in the channels, this is illustrated in figure 5.4. The velocity is plotted on a plane section in the middle of the channel height for three different channel widths and these behaviours agree with the Darcy-Weisbach pressure drop equation (2.10), where an increase in velocity or decreased channel width will increase the pressure drop.

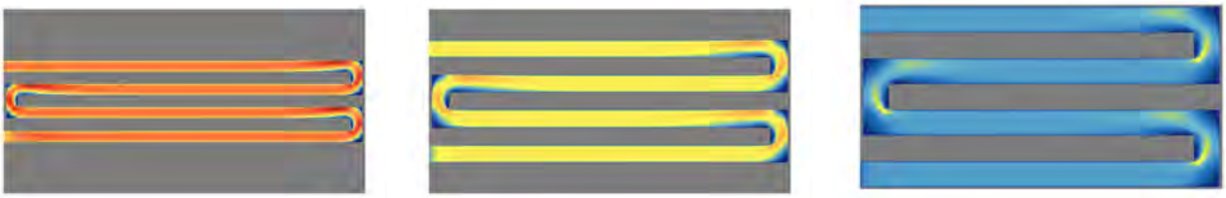

(a) Channel width 12 mm *(b) Channel width 18 mm* *(c) Channel width 26.5 mm*

Figure 5.4: Fluid velocity plots for different channel widths, multiple cooling plates

The low variance in pressure drop for the large plate designs, shown in table 4.1, is due to the changing number of channels when the channel width is altered. Resulting in the mass flow being distributed over more channels, leading to a decreased velocity. While narrower channels increases the velocity. A combination of these two effects results in a relatively constant velocity in the channels for the different widths, as displayed in figure 5.5. This leads to a relatively constant pressure drop since the velocity is squared in the pressure drop equation (2.10).

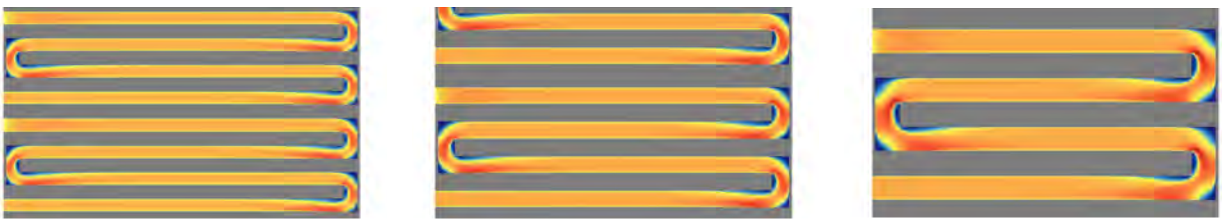

(a) Channels width 14 mm *(b) Channels width 18 mm* *(c) Channels width 26.5 mm*

Figure 5.5: Fluid velocity plots for different channel widths, large cooling plate

The large cooling plate with 18 *mm* channels has a lower interface area than its neighbouring designs, see table 4.1. The reason behind this is that the particular channel width resulted in narrower channels however not enough additional channels could be fitted within the dimensions of the cooling plate to counteract the decreased channel width, resulting in a lower interface area.

5.2 Further Processed Multiple Plate Designs

Areas of improvement were found for the original Triple U design. For instance, the pressure drop could be decreased since there was room to widen the channels. Widening of the channels would also lead to a larger interface area between the coolant and the aluminium. A surface temperature plot of the original Triple U design is shown in figure 5.6. Since there is generally a lot of aluminium and less coolant, the inlet portion of the plate becomes very cool relative to the rest of the plate. The outlet portion of the plate also becomes very hot relative to the inlet portion of the plate.

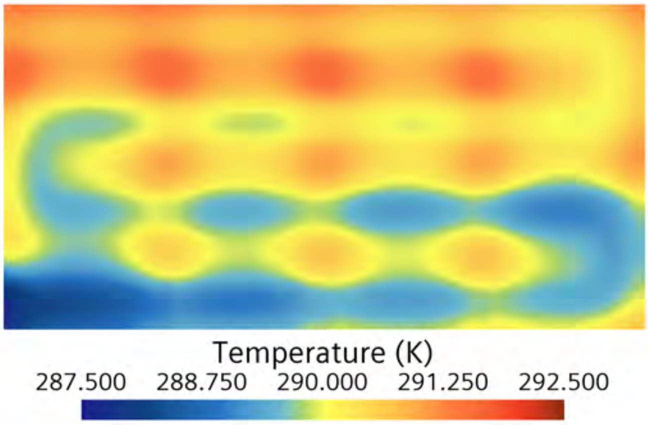

Figure 5.6: Triple U: Temperature plot of the cooling plate surface

Because the Triple U design had room to widen the channels, a widened version of the Triple U design was created, called the Wider Triple U design. With a larger interface area between the coolant and the aluminium more heat transfer could take place. The maximum volume averaged battery cell temperature was lowered from 305.3 K to 304.9 K. The pressure drop was also decreased from 141 129 Pa to 83 461 Pa. However a negative consequence of this design was that the temperature difference was actually increased from 0.403 K to 0.529 K, for the same mass flow of 40 l/min. This is seen in figure 5.7, where the plate is generally hotter further from the inlet. Since the Wider Triple U design managed to decrease the maximum temperature and pressure drop of the system it was investigated if it could be decreased even further by increasing the contact area of the coolant and aluminium.

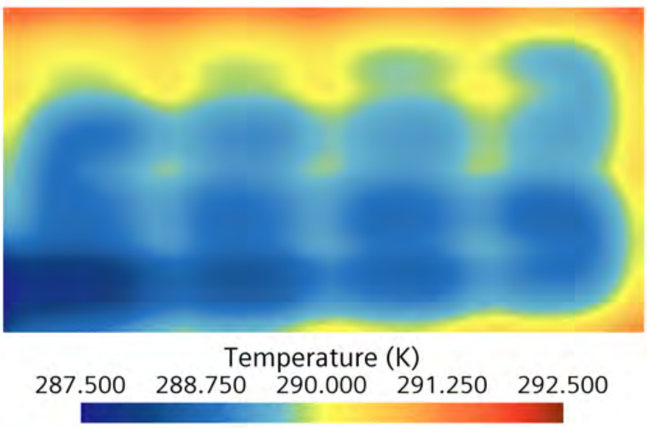

Figure 5.7: Wider Triple U: Temperature plot of the cooling plate surface

This led to the Single U channel design. Using a single channel allowed for the channel to be much wider and shorter indicating a lower pressure drop. However, in order to retain structural rigidity, some supportive walls were added inside the channels. The walls were kept thin to maintain a large contact area between the coolant and the aluminium plate. This design yielded a maximum temperature of 305.0 K as compared to the original Triple U 305.3 K. The pressure drop was also much lower at 22 135 Pa. Meaning that the pressure drop was reduced from 141 129 Pa to 22 135 Pa, a decrease of $\approx 85\%$. However the Single U design performed worst in terms of temperature difference, where it yielded a maximum temperature difference of 0.726 K. In the results of the Single U channel design it became very apparent that there was a cold zone near the inlet and a hot zone furthest from the inlet, as shown in figure 5.8.

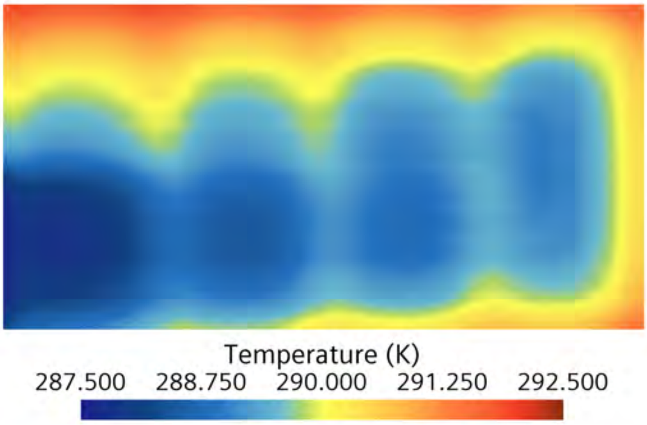

Figure 5.8: Single U: Temperature plot of the cooling plate surface

Further optimisation of the Single U design is possible, which is illustrated in figure 5.9a where the fluid temperature is plotted in the middle of the channel height. The fluid in the outermost channel reaches a considerably higher temperature than the innermost channel. This could be improved by changing the width of the channels to increase the mass flow in the outer channel. More flow in the outer channel would decrease the temperature difference by cooling the battery cell row furthest from the inlet more, which is the largest drawback of this design. More flow in the outer channel is achieved by making the inner channels narrower to increase the flow resistance in those channels. A surface plot of the velocity for the single U design is displayed in figure 5.9b. The velocity in the innermost channel is generally about double the velocity of the outermost channel.

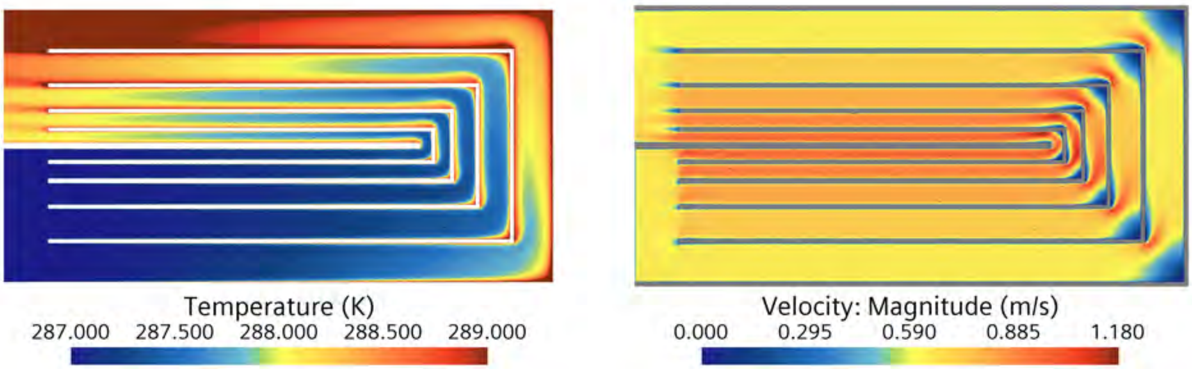

(a) Temperature *(b) Velocity*

Figure 5.9: Plane section surface plots of the Single U design

By finding that there was a hot zone furthest from the inlet it was investigated if the hot temperatures from the hot zone could be spread more evenly to the colder inlet side of the battery pack. This result gave rise to the Five U design, where the idea was to mix some of the heat from the hot side to the cold side by making more U-turns and thereby minimizing the heat concentrations. The Five U design consists of narrower channels to make room for 5 U-turns, the additional turns resulted in a longer channel. This led to the temperature mixing very well as shown in the surface temperature plot in figure 5.10. The pressure drop did however increase substantially. This is attributed to the pressure drop being a function of the cross-sectional area and length of the channels. The pressure drop for the Five U design was 206 010 Pa, an increase from the 141 129 Pa of the original Triple U design. The temperature difference was however decreased to 0.337 K, the lowest temperature difference in the battery pack thus far. It is clear from the temperature plot in figure 5.10 that the majority of the heat flux is now more spread out across the surface of the plate and not only concentrated on the inlet side.

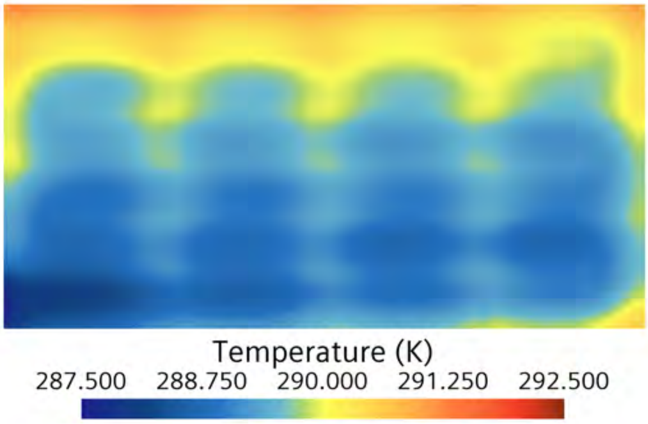

Figure 5.10: Five U: Temperature plot of the cooling plate surface

Lastly it was investigated if the Wider Triple U design could be improved by adding 1 mm wide fins throughout the channel. The addition of fins yielded only a minuscule increase in contact area, which also became clear in the results where the Wider Triple U and Wider Triple U with fins performed similarly. A plot of the plate temperature is displayed in figure 5.11 and shows great similarities to the Wider Triple U design.

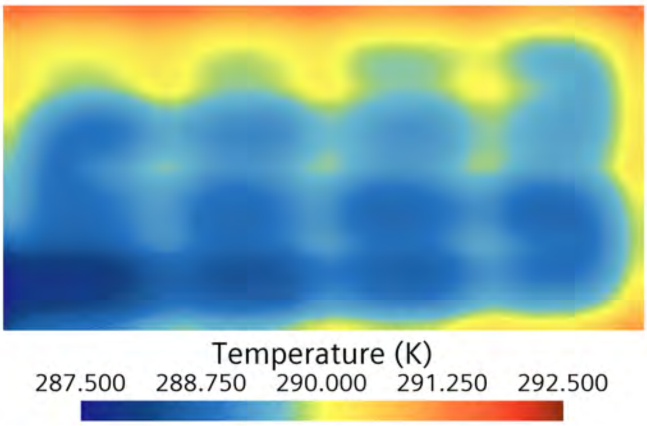

Figure 5.11: Wider Triple U with fins: Temperature plot of the cooling plate surface

Compared to the Wider Triple U design the effect of adding fins on the coolant flow is minimal. Velocity plots for both Wider Triple U designs are presented in figure 5.12. The flow around the fins creates small wakes. Resulting in a small pressure drop increase of 1938 Pa, as seen in table 4.4.

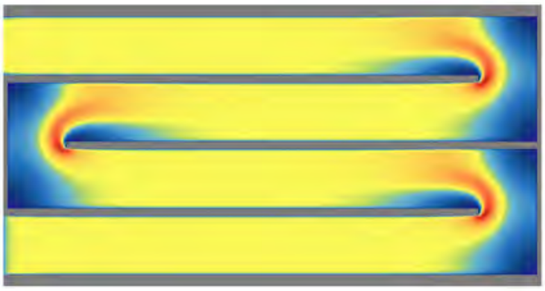

(a) Wider Triple U without fins

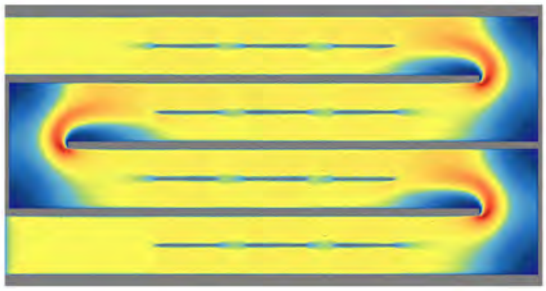

(b) Wider Triple U with fins

Figure 5.12: Plane section surface plots of the fluid velocity

5.3 Transient simulations

Through the transient simulations in section 4.6 it was shown that the heating and cooling of the battery cells took a considerable amount of time. For the unsteady simulation to reach steady state, starting every region from the inlet temperature 287 K, it took roughly 3600 seconds. When the battery pack heat generation was cut in half it took roughly 4000 seconds for the cooling system to cool the battery cells to their new lower maximum temperatures. Lowering of the battery volumetric heat source also caused the temperature difference to drop from 0.399 K to 0.301 K. Indicating that the total amount of heat generated by all battery cells has an impact on the temperature difference in the battery pack. From the crisis simulation it became apparent that the cooling system managed to cool the battery pack and also at a shorter time than it took for the battery pack to overheat.

From the transient simulations a conclusion is drawn that the unsteady solution eventually corresponds to the steady-state solution and that the time it takes for the battery pack to heat and cool is fairly long.

5.4 Evaluating the best design

Judging by the pressure drop versus maximum T and pressure drop versus temperature difference plots in figure 5.13a and 5.13b it is hard to draw any hard conclusions on what is the best design, the different designs are good in their own respects. In terms of pressure drop vs temperature difference, all designs except Single U perform similarly at similar pressure drops. At the maximum flow rate of 40 l/min, i.e. at the highest pressure drop, the temperature difference is already at 0.726 K for the single U design, way above the rest of the designs. However from the pressure drop versus maximum temperature plot, it is very apparent that it is much cheaper in terms of pressure drop to get a much lower maximum temperature for the Single U design. The Single U design is therefore good at keeping the battery pack cool, at much lower pressure drops, but not as effective at distributing the heat evenly.

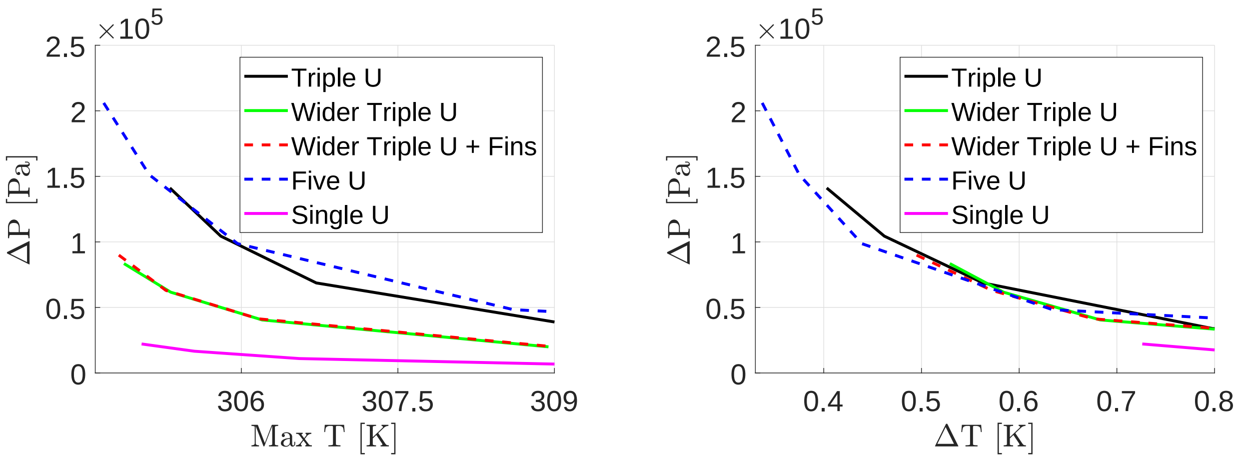

(a) Pressure drop versus maximum temperature

(b) Pressure drop versus temperature difference

Figure 5.13: Results for varying volume flow rates

If high pressure drops is not an issue for an application then the Five U design yields the best overall performance. For a higher pressure drop it yields the lowest temperature difference of 0.337 K and also the lowest maximum temperature of 304.7 K.

Comparing the designs at similar pressure drops yields a more fair comparison since the pressure drop is the running cost of the design. At pressure drops ranging from 45 kPa to 80 kPa the temperature difference varies roughly from 0.5 K to 0.7 K for all multiple plate designs, except the single U design. In this region of pressure drops the Wider Triple U and Wider Triple U with fins perform the best in terms of maximum temperature.

A reiteration of the whole discussion and the comparison of the performance across the board for all designs is shown in table 5.1. It seems that a trade-off between a low temperature difference and a low pressure drop is necessary, one can not have both at the same time. Generally where a low pressure drop is seen a high temperature difference is present and vice versa.

Table 5.1: Designs and performance metrics, at the maximum flow rate

Design	**ΔT**	**Max T**	**ΔP [Pa]**
Triple U	low	low	high
Wider Triple U	high	low	low
Wider Triple U with fins	high	low	low
Five U	low	low	high
Single U	high	low	low

5.5 Limitations of the used battery cell design

The simulated battery cell design has an anisotropic thermal conductivity, with the low conductivity in the normal direction of the cooling plates, counteracting the effectiveness of the multiple cooling plate design. This is illustrated in figure 5.14a which shows large temperature gradients on the battery cell surfaces in the normal direction of the cooling plate. Figure 5.14a is zoomed in on the first couple of rows of battery cells, viewing the cells from the top. Rotating the battery cells 90 degrees or redesigning the internals of the battery cells increases the heat transfer from the battery cells. This relocates the large temperature gradients to the normal direction of the foam, illustrated in figure 5.14b. Resulting in lower battery pack temperatures and lower battery cell temperature differences. The maximum battery cell temperature was lowered by 2.5 K and the temperature difference was lowered by 0.08 K compared to the original Triple U design.

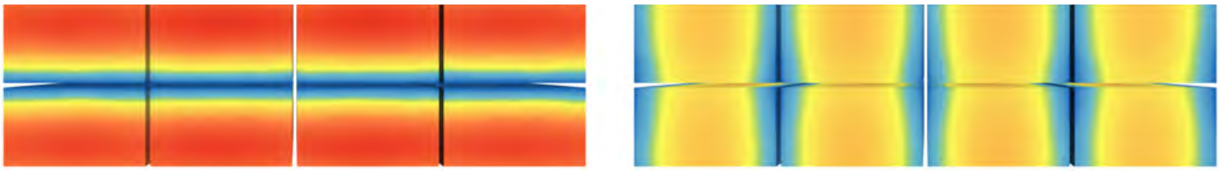

(a) Regular battery cells *(b) Changed anisotropic thermal conductivity*

Figure 5.14: Temperature plots of battery packs

5.6 Automatic Optimisation & Methodology

The automatic optimisation proved to be very useful. Fully automating every step of the simulation work allowed for easy parameterization of the geometry, flow rate and the inlet temperature just to name a few. This allowed for a lot of results to be acquired with little to no input. The presented results shows that it was possible to minimize the temperature difference, maximum battery cell temperature and pressure drop using the methodology defined in the flowchart in figure 1.2. It is still beneficial to make sure that the simulation has converged and that all results are mesh independent.

In the optimisation work applied in this thesis one part was automatic and the other was not. For the automatic script the input is a parameterised geometry and in this thesis it was applied on the initial designs of the two cooling configurations. The script yielded results for varying channel widths regardless if the result yielded a lower temperature difference or not. It is up to the user to define how the geometry should be varied and the optimisation criteria. The automatic optimisation could also be implemented on the further processed multiple plate designs but instead testing new designs was prioritised.

5.7 Limitations of the study

The 5000 W heat generation of the battery pack is sort of a worst-case scenario used to investigate the performance of the cooling plate configurations. For more lifelike results it would be beneficial to also simulate the inner electrochemistry of the batteries and thereby yield better results.

The heat flux out through the foam was only a qualified guess. This parameter is highly dependent on the ambient conditions. If it is hotter outside the battery pack than inside, heat would in reality flow in the other direction. It was chosen to be 10 W/m^2 out of the system so as to not cool the system too much relative to the implemented cooling system and not too little as to not make a difference. 10 W/m^2 yields a total boundary heat flux of roughly 21.89 W. Since the battery pack generates 5000 W the flow through the foam is only a very small part of the energy equilibrium.

The used contact resistance between the different interfaces is assumed to be valid enough for this study but do not agree fully with real-life scenarios.

6 Conclusion

In this thesis it was investigated what cooling plate configuration had the best cooling performance. Parameters for what constitutes the best cooling performance were also investigated. A good cooling performance provides low temperature differences between the battery cells in the battery pack to even out the expected lifespan of all battery cells. A good cooling performance also ensures that the battery cells operate within the optimal temperature range for the lithium-ion battery cells. Higher temperatures lead to accelerated wear of the battery cells. It was found that placing cooling plates in between the battery cells was a more effective configuration for cooling the battery cells and ensuring an even temperature distribution in the battery pack. This configuration will prevent extended uneven battery wear and thermal runaway. The other configuration, which cools the battery pack from the bottom, resulted in a uneven battery wear and a large risk of thermal runaway.

The dominating variable in the amount of heat transfer that could occur was found to be the interface area between the coolant and the cooling plate. By having a large interface area more heat transfer could occur. The design of the cooling channels was found to have the most impact on the temperature difference. Therefore a design with a large interface area and long channels was found to yield both low temperatures and low temperature differences in the battery pack.

The channel design also had a large impact on the pressure drop. Longer channels attributes to higher pressure drops, whereas wider channels result in lower pressure drops. The pressure drop is also controlled by the mass flow rate of the coolant. Comparing the multiple cooling plate designs at similar pressure drops gives an indication of what design is most effective at cooling the system per pressure drop. The Five U Design yields the lowest temperatures and temperature differences but at the cost of the highest pressure drop. The Wider Triple U design yields similar maximum temperatures in the battery pack and a small increase in temperature difference in the battery pack but at less than half the pressure drop of the Five U design.

The automatic optimisation methodology streamlines the optimisation work by letting the computer do the work. Through parameterisation and preparing the simulation using Java macros little to no input is needed by the user to yield a lot of results. For these simple designs, using only rectangular blocks, the design could be parameterised and run using different channel widths and fluid conditions.

6.1 Future Work:

Simulating the electrochemistry of the batteries would yield more realistic results. In this study the battery cells were set up as rectangular blocks with a volumetric heat source to simulate a worst-case scenario of a lot of heat added to the system.

Heat flux to or from the ambience should be more thoroughly investigated to get more lifelike results.

For the thermal contact resistance physical experiments can be made using material samples or the contact resistance can be modelled to further improve the thermal contact resistance. The thermal contact resistance can be lowered by using a thermal interface material to improve the conductance.

It has not been investigated if there are any auxiliary systems that manages to cool the coolant enough for it to always be at 287 K and 40 l/min at the inlet. Since the coolant flows in a closed-loop system the hot coolant at the outlet must somehow be cooled before re-entering the cooling system at the inlet. The chosen 287 K was chosen as a qualified guess. Since the maximum temperature of the battery cells is linearly dependent on the inlet temperature of the coolant, this should be investigated further.

The automatic optimisation methodology can be improved by implementing a mesh convergence check since that was something that had to be done manually to make sure the solutions were mesh independent. Moreover it could also be made available for more advanced designs, using rounded corners for example.

Bibliography

[1] E, Helmers., P, Marx. "Electric cars: technical characteristics and environmental impacts." *Environmental Sciences Europe*, vol. 24, no. 14, 2012. [Online] Available: https://doi.org/10.1186/2190-4715-24-14

[2] M. Barisione, "Electric vehicles and air pollution: the claims and the facts," European Public Health Alliance, [Online], Mar. 5, 2021. Available: https://epha.org/electric-vehicles-and-air-pollution-the-claims-and-the-facts/

[3] J. Partridge, "Electric cars 'will be cheaper to produce than fossil fuel vehicles by 2027'" The Guardian, May 9, 2021. [Online] Available: https://www.theguardian.com/business/2021/may/09/electric-cars-will-be-cheaper-to-produce-than-fossil-fuel-vehicles-by-2027

[4] S. Edelstein, "EVs will still cost more to make, even after batteries get much cheaper" Green Car Reports, September 2, 2020. [Online] Available: https://www.greencarreports.com/news/1129461_evs-cost-more-to-build-even-after-batteries-get-cheaper

[5] D. P. Finegan et al, "*In-operando* high-speed tomography of lithium-ion batteries during thermal runaway", *Nature Communications*, vol. 6, no. 6924, 2015, [Online] Available: https://doi.org/10.1038/ncomms7924

[6] "What's the Difference Between EV Charging Levels?", FreeWire Technologies, Jul. 1, 2020. [Online] Available: https://freewiretech.com/difference-between-ev-charging-levels/

[7] M. Winter, R. J. Brodd, "What Are Batteries, Fuel Cells, and Supercapacitors?," *Chemical Reviews*, vol. 104, no. 10, pp. 4245-4270, Sep. 28, 2004. [Online] Available: https://doi.org/10.1021/cr020730k

[8] P. Miller, "Automotive Lithium-Ion Batteries," *Johnson Matthey Technology Review*, vol. 59, no. 1, pp.4-13, Jan. 2015. [Online] Available: https://doi.org/10.1595/205651315X685445

[9] S. Ma et al, "Temperature effect and thermal impact in lithium-ion batteries: A review". *Progress in Natural Science: Materials International*, vol 28, issue 6, pp. 653-666, Dec. 2018. [Online] Available: https://doi.org/10.1016/j.pnsc.2018.11.002.

[10] J. S. Edge et al, "Lithium ion battery degradation: what you need to know," *Physical Chemistry Chemical Physics*, vol. 23, issue 14, pp. 8200-8221, 2021. [Online] Available: http://dx.doi.org/10.1039/D1CP00359C

[11] "Trace Degradation Analysis of Lithium-Ion Battery Components," *R&D*, Apr. 22, 2014. Accessed on: Jan. 26, 2022. [Online] Available: https://www.rdworldonline.com/trace-degradation-analysis-of-lithium-ion-battery-components/

[12] Q. Wang, P. Ping, X. Zhao, G. Chu, J. Sun, C. Chen, "Thermal runaway caused fire and explosion of lithium ion battery," *Journal of Power Sources*, vol. 208, pp. 210-224, Jun. 15, 2012. [Online] Available: https://doi.org/10.1016/j.jpowsour.2012.02.038

[13] J. Kim, J. Oh, H. Lee, "Review on battery thermal management system for electric vehicles," *Applied Thermal Engineering*, vol 149, pp. 192-212, Feb. 2019.[Online] Available: https://doi.org/10.1016/j.applthermaleng.2018.12.020

[14] H. K. Versteeg, W. Malalasekera, *An Introduction to Computational Fluid Dynamics*, 2nd ed., Pearson Education Limited, 2007.

[15] M. J. Ketabdari, H. Saghi and H. Rezaei, "Comparison of Staggered and Collocated grids for solving Navier-Stokes Equations," 5th National Congress on Civil Engineering, May. 2010. [Online] Available: http://confnews.um.ac.ir/images/41/conferences/5ncce/1525.pdf

[16] F. White, *Fluid Mechanics*, 8th ed., New York NY: McGraw-Hill Education, 2016.

[17] J.P. Holman, *Heat Transfer*, 8th ed., New York NY: McGraw-Hill Education, 1997.

[18] A. Zaharia. "Passive Cooling vs. Active Cooling – What's the Difference?," *SimScale Blog*, Jun. 14, 2021. [Online]. Available: https://www.simscale.com/blog/2017/01/active-and-passive-cooling/

[19] "Electric Car 101: Liquid vs. Air Battery Cooling Systems," *GigaOm*, Sep. 29, 2010. [Online]. Available: https://gigaom.com/2010/09/29/electric-car-101-liquid-vs-air-battery-cooling-systems/

[20] W. Wu, S. Wang, W. Wu, K. Chen, S. Hong and Y. Lai, "A critical review of battery thermal performance and liquid based battery thermal management". *Energy Conversion and Management*, vol 182, pp. 262-281, Feb. 2019., [Online] Available: https://doi.org/10.1016/j.enconman.2018.12.051

[21] B. Pause, "Phase change materials and their application in coatings and laminates for textiles," in *Smart Textile Coatings and Laminates*, W. Smith, Ed., Woodhead Publishing, 2010, ch. 9, pp. 236-250. [Ebook] Available: https://doi.org/10.1533/9781845697785.2.236

A Mesh Study

Table A.1: Mesh Study Solid Regions

Number of cells	Max T [K]	Base size Foam and Plate [m]
24 519 795	305.266	0.01
20 743 330	305.259	0.02
17 676 746	305.254	0.04
17 244 671	305.175	0.06
17 107 456	305.139	0.08

Table A.2: Mesh Study large plate

Number of cells	Pressure drop [Pa]	Max T [K]	Base size coolant [m]
31 088 830	359 744	328.229	0.005
8 920 697	359 926	328.265	0.01
3 561 321	360 043	328.286	0.02
2 423 785	360 479	328.321	0.03
1 986 089	361 117	328.283	0.04

Table A.3: Mesh Study multiple plates

Number of cells	Pressure drop [Pa]	Max T [K]	Base size coolant [m]
17 676 746	141 584	305.254	0.01
6 314 558	141 125	305.283	0.02
4 826 446	141 106	305.285	0.025
3 853 382	141 085	305.275	0.03
2 918 022	141 010	305.269	0.04
2 343 050	140 913	305.299	0.05

Table A.4: Mesh Study Wider Triple U

Number of cells	Pressure drop [Pa]	Max T [K]	Base size coolant [m]
25 516 540	83 722	304.857	0.01
8 379 308	83 461	304.875	0.02
4 682 360	83 171	304.851	0.03
3 342 692	83 265	304.805	0.04

Table A.5: Mesh Study Single U design

Number of cells	Pressure drop [Pa]	Max T [K]	Base size coolant [m]
35 224 351	22 200	305.027	0.01
11 480 455	22 136	305.044	0.02
6 519 501	22 077	305.057	0.03
4 822 493	22 083	305.034	0.04

Table A.6: Mesh Study Five U

Number of cells	**Pressure drop [Pa]**	**Max T [K]**	**Base size coolant [m]**
25 992 790	207 112	304.649	0.01
9 023 726	206 011	304.681	0.02
5 491 500	204 963	304.672	0.03
4 055 197	205 124	304.636	0.04

B Study of Wall y+

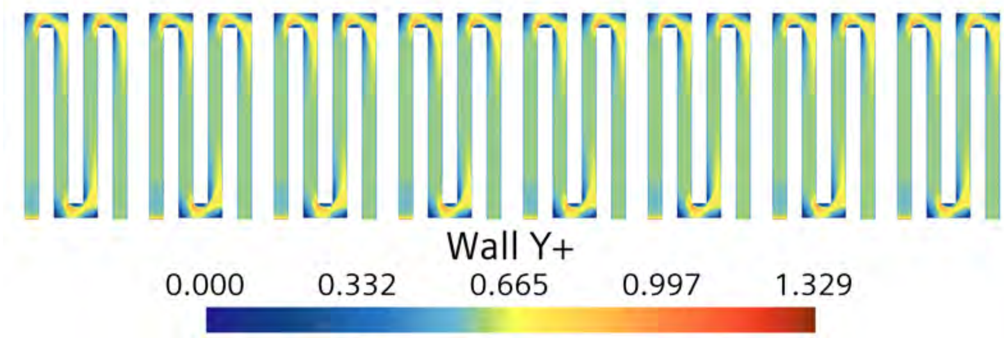

Figure B.1: Plot of y+ large cooling plate

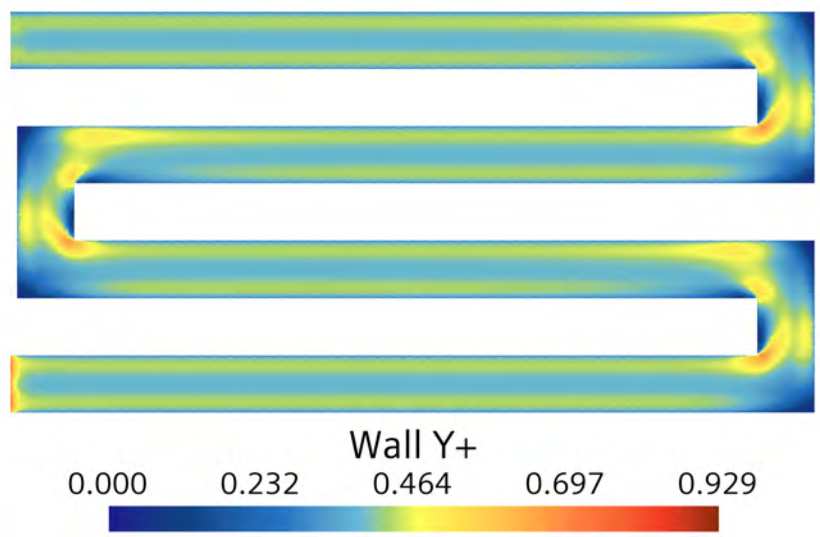

Figure B.2: Plot of y+ multiple cooling plate Triple U design

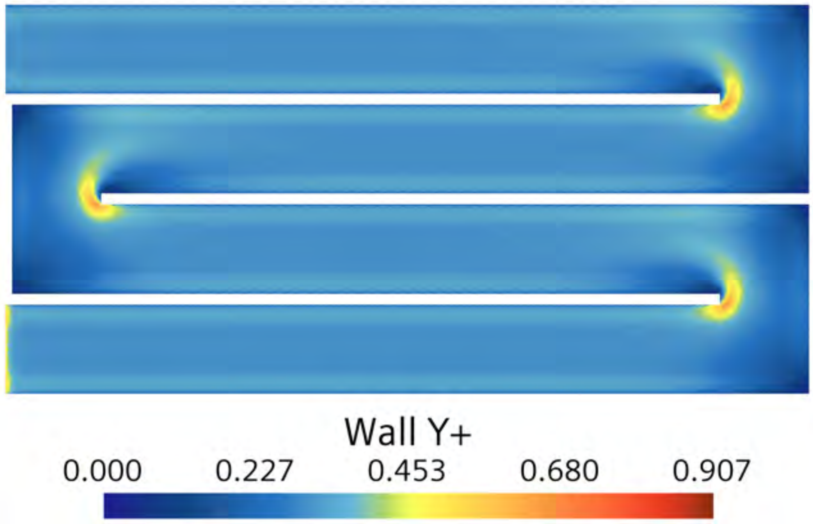

Figure B.3: Plot of y+ multiple cooling plate Wide triple U design

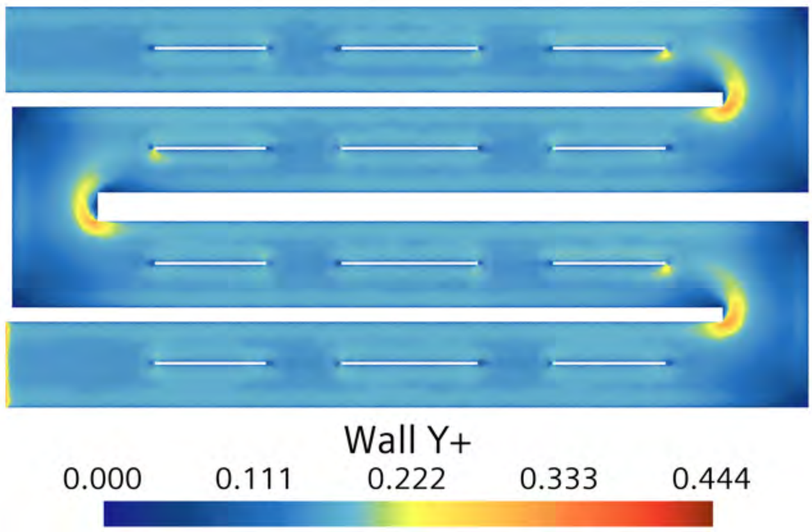

Figure B.4: Plot of y+ multiple cooling plate Wide with fins triple U design

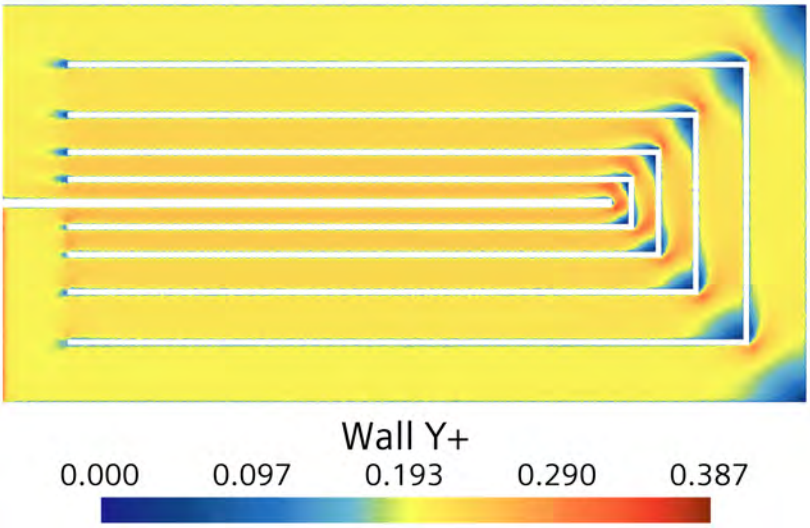

Figure B.5: Plot of y+ multiple cooling plate Single U design

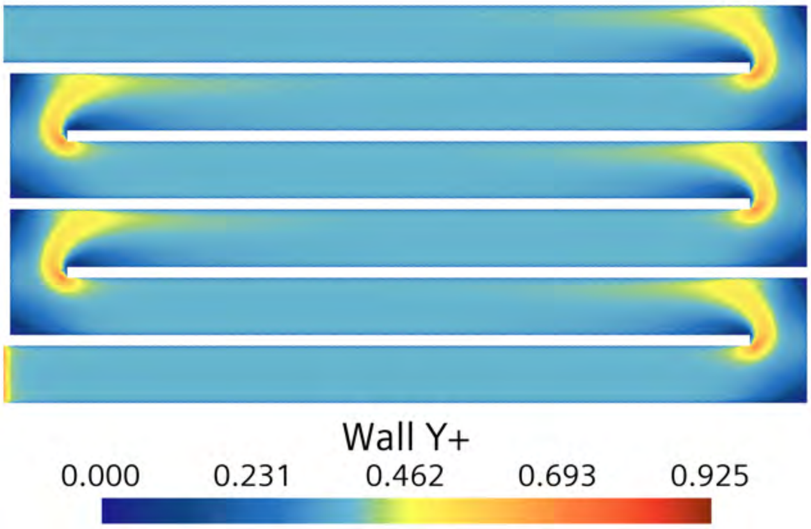

Figure B.6: Plot of y+ multiple cooling plate Five U design

DEPARTMENT OF MECHANICS AND
MARITIME SCIENCES
CHALMERS UNIVERSITY OF TECHNOLOGY
Gothenburg, Sweden 2022
www.chalmers.se

CHALMERS
UNIVERSITY OF TECHNOLOGY